Bachelor Project

Czech Technical University in Prague

F3

Faculty of Electrical Engineering

Improving control system parameters to optimize electric energy use in microgrid

Leon Gritsyuk

Supervisor: Ing. Josef Černohous
Supervisor–specialist: Ing. Oleksij Čumak, Ph.D.
Field of study: Electrical Engineering, Power Engineering and Management
May 2024

ZADÁNÍ BAKALÁŘSKÉ PRÁCE

I. OSOBNÍ A STUDIJNÍ ÚDAJE

Příjmení: **Gritsyuk** Jméno: **Leon** Osobní číslo: **507420**

Fakulta/ústav: **Fakulta elektrotechnická**

Zadávající katedra/ústav: **Katedra ekonomiky, manažerství a humanitních věd**

Studijní program: **Elektrotechnika, energetika a management**

Specializace: **Elektrotechnika a management**

II. ÚDAJE K BAKALÁŘSKÉ PRÁCI

Název bakalářské práce:

Zlepšení parametrů řídícího systému pro optimalizaci spotřeby elektrické energie v mikrosíti

Název bakalářské práce anglicky:

Improving control system parameters to optimize electric energy use in microgrid

Pokyny pro vypracování:

1. Proveďte rešerši metod pro řízení mikrosíti.
2. Popište současné parametry výkonových zařízení v mikrosíti a sestavte energetickou bilanci mikrosítě.
3. Navrhněte vhodné řešení pro měření parametrů při řízení mikrosítě a implementujte toto řešení v mikrosíti.
4. Vyhodnoťte ekonomický přínos implementace nového řízení mikrosítě.

Seznam doporučené literatury:

R. Lasseter, Microgrids in 2002
T. Dragicevic, “Advanced lvdc electrical power architectures and microgrids
N. Hatziargyriou, Microgrids
Brealey R., Myers S., Allen F.: Principles of Corporate Finance

Jméno a pracoviště vedoucí(ho) bakalářské práce:

Ing. Josef Černohous CVUT v Praze FEL K13116

Jméno a pracoviště druhé(ho) vedoucí(ho) nebo konzultanta(ky) bakalářské práce:

Datum zadání bakalářské práce: **15.02.2024** Termín odevzdání bakalářské práce: _____

Platnost zadání bakalářské práce: **21.09.2025**

Ing. Josef Černohous podpis vedoucí(ho) práce	podpis vedoucí(ho) ústavu/katedry	prof. Mgr. Petr Páta, Ph.D. podpis děkana(ky)

III. PŘEVZETÍ ZADÁNÍ

Student bere na vědomí, že je povinen vypracovat bakalářskou práci samostatně, bez cizí pomoci, s výjimkou poskytnutých konzultací. Seznam použité literatury, jiných pramenů a jmen konzultantů je třeba uvést v bakalářské práci.

. _____
Datum převzetí zadání

_____
Podpis studenta

Acknowledgements

Foremost expressions of gratitude are earnestly conveyed to my esteemed parents, whose unwavering support has been a cornerstone throughout the entirety of this scholarly pursuit. Profound acknowledgment is equally extended to Eaton for graciously affording me the enriching opportunity to engage in the endeavors of this project. Moreover, heartfelt appreciation is tendered to Ing. Oleksij Chumak, Ph.D., Ing. Tomáš Kralík, Ph.D., and Ing. Josef Černohous for their benevolent dispensation of sagacity and erudition, which significantly enriched the course of my scholarly odyssey.

Declaration

I declare that this work is all my own work and I have cited all sources I have used in the bibliography.

Prague, May 24, 2024

Prohlašuji, že jsem předloženou práci vypracoval samostatně, a že jsem uvedl veškerou použitou literaturu.

V Praze, 24. května 2024

Abstract

Rising global demand in switching to carbon neutrality and ensuring safer energy has led to the appearance of a promising technological concept called DC microgrid (DC MG). One of the key issues in the DC MGs is power sharing instability, which is being addressed by different control techniques. Most of those approaches utilize electrical measurements to achieve stability. The measurements' cleanness and stability will be addressed in this bachelor project by implementing a discrete filter and voltage drop compensation algorithm into the DC MG's control system and subsequently testing it in a real DC MG. Moreover, the economical analysis of a new theoretical optimization control will be provided.

Keywords: Direct Current Microgrid, Voltage Drop Compensation, Simulation, FIR Filter

Supervisor: Ing. Josef Černohous

Abstrakt

Rostoucí globální poptávka po přechodu na uhlíkovou neutralitu a zajištění bezpečnější energie vedlo ke vzniku slibného technologického konceptu s názvem DC microgrid (DC MG). Jedním z klíčových problémů V DC MG je nestabilita rovnováhy výkonu, která je řešena různými kontrolními technikami. Většina těchto přístupů využívá elektrická měření pro dosažení stability. Čistota měření a stabilita bude v tomto bakalářském projektu řešena implementací diskrétního filtru a algoritmu kompenzace úbytku napětí do řídicího systému DC MG a následném testováním v reálném DC MG. Navíc ekonomická analýza nového teoretického optimalizačního řízení bude poskytnuta.

Klíčová slova: Direct Current Microgrid, Kompenzace Ubytku Napětí, Simulace, FIR Filtr

Překlad názvu: Zlepšení parametrů řídícího systému pro optimalizaci spotřeby elektrické energie v mikrosíti

Contents

Chapter 1
Introduction

As the world nowadays faces such problems as climate change caused by carbon emissions[1], little amount of affordable and sustainable alternatives to fossil-fuel electricity generation[2, 3] and a strive to improve energy efficiency[4], more financial resources are invested into the development of new technologies, which can potentially help humanity by speeding up the process of resolving those problems. One of such technologies, which is being examined and explored around the globe, is smart-grids (SG). SG is a concept aimed at modernizing the electrical power grid through the utilization of sophisticated automated control, communication methods, and various information technology resources[5]. Alongside improvements made in power electronics related to direct current (DC) voltage regulations[6], one type of SG, DC microgrid (MG) (DC microgrid (DC MG)), received a pivotal role in a global research community. Since MG is a relatively new concept, presented around two decades ago[7], there is still plenty of room for improvements and adjustments to be addressed until DC MG becomes as commonly used as alternating current (AC) grids today. For instance, one of the issues present in today's DC MGs, which incorporate control algorithms based on electrical measurements, is instability[8, 9]. Such instability can cause DC MG to operate inefficiently and unexpectedly, causing unreliability and higher operational costs. By establishing measurements' stability, DC MG can receive a step forward toward becoming a promising way of achieving carbon neutrality and improving energy efficiency.

1.1 Goal

The primary objective of this thesis is to devise an algorithm designed to analyze voltage drops within DC microgrids at the software level. This endeavor is motivated by the imperative to enhance the operational stability and reliability of DC microgrid systems, thereby minimizing the occurrence of faults and optimizing overall performance. Central to this endeavor is the development of a sophisticated algorithm capable of identifying and compensating for voltage drops within the microgrid infrastructure. By leveraging computational techniques, the algorithm aims to accurately assess voltage variations and implement corrective measures in real-time, thus ensuring the

seamless operation of the microgrid under varying load conditions. Furthermore, the implementation of filtering mechanisms represents a pivotal aspect of this study, aimed at refining the accuracy and reliability of measurement inputs utilized in the droop control of the microgrid. By filtering out extraneous noise and erroneous data, the filtering process endeavors to furnish the droop control system with precise and dependable information, thereby fostering greater stability and resilience within the microgrid network. In addition to technical considerations, this thesis also undertakes an economic analysis to evaluate the viability and efficacy of a new theoretical control method for optimizing energy use in the DC MG. Through the application of financial methods and metrics, the economic feasibility of deploying the method is assessed. Moreover, particular emphasis is placed on the theoretical application of the algorithm for peak-shaving, with a view towards optimizing energy utilization and minimizing operational costs within the microgrid infrastructure. By integrating technical innovation with economic scrutiny, this thesis endeavors to provide a comprehensive framework for the development and implementation of a robust voltage drop compensation algorithm in DC microgrid systems. Through the synthesis of computational prowess, filtering techniques, and economic evaluation, this study aims to contribute towards the advancement of sustainable and resilient energy solutions in the realm of DC microgrid technology.

1.2 Structure

This bachelor's project will encompass several chapters. The second chapter will have a theoretical introduction to the topics that are utilized in the project, such as a more detailed explanation of the MGs, what algorithms exist in the field of stabilization and control, necessary measurements that are required for the solution, and a simulation tool. The comprehensive process of a problem-solving process and its implementation in the real DC MG will be shown in the third chapter. The fourth part will analyze the theoretical implementation of an optimizing method from the economic point of view, including operational costs and energy consumption. In the fifth chapter a conclusion about both technical and economic results will be given. A noteworthy mention should additionally be given, that this study incorporates outputs provided by ChatGPT 3.5[10]. The mentioned artificial intelligence was solely used for checking grammar and paraphrasing.

Chapter 2

Theoretical Foundation

This chapter will provide a thorough foundation for the topics which are important for this study, such as what is a microgrid (MG), what are main components in the MG, what control techniques exist in the industry.

2.1 Distributed Energy Resources

Before diving into the explanation of what is the microgrid, it is crucial to acquire an understanding of distributed energy resources (DER). DER refers to electric power generation resources which are directly interconnected with low voltage (LV) or medium voltage (MV) distribution systems, instead of bulk power transmission systems. DER include both as units capable of generating power, and units capable of storing energy. Figure 2.1 represents technologies' structure of DER[11].

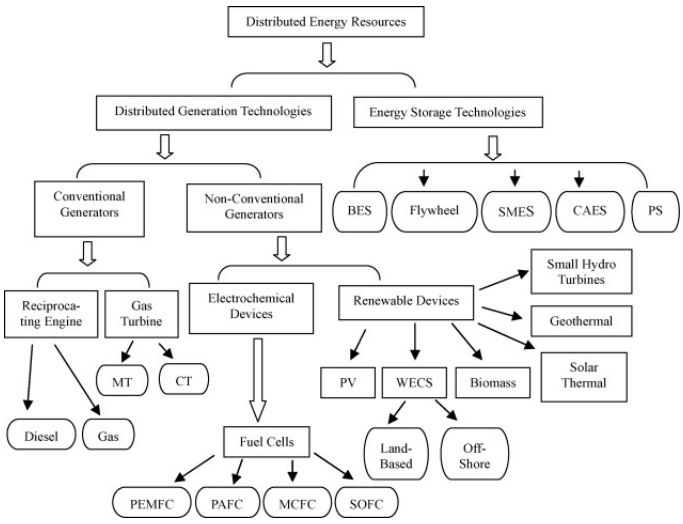

Figure 2.1: DER technologies[11].

A prime example of DER capable of generating power is photovoltaic (PV) technology. PV systems convert sunlight directly into electricity, making them an environmentally friendly and sustainable choice for decentralized energy production. The battery energy storage system (BESS) is an another

noteworthy example. BESS stores excess energy generated by sources like PV systems or wind turbines. It plays a crucial role in balancing supply and demand, enhancing grid stability, and providing backup power during outages.

2.1.1 Photovoltaic Technology

Although solar energy holds great promise as an alternative to fossil fuel combustion, the technology for effectively harnessing this energy is still undergoing constant development and improvement. The rapidly advancing field of photovoltaic technology is considered a compelling means of utilizing solar energy[12]. PV technology operates by converting sunlight into electricity through the use of semiconductors[13]. The working principle of a solar cell is based on the photoelectric effect, depicted in Figure 2.2.

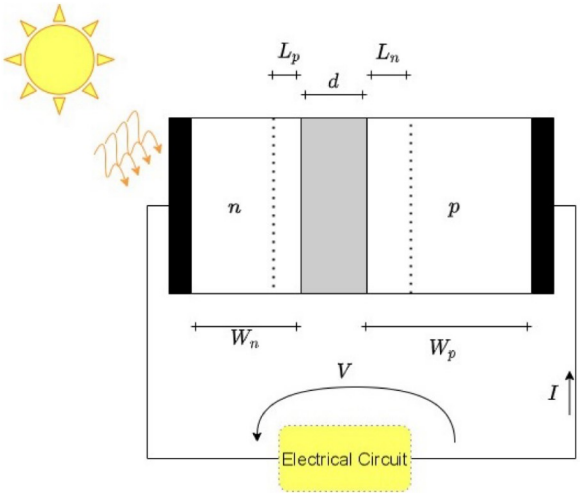

Figure 2.2: Diagram of a p-n junction solar cell[14].

When the sunlight strikes the solar cell, electrons are being ejected from the semiconductor[14]. Various photovoltaic effects can be distinguished and classified based on the source of the local electrical fields. With the reference to the Figure 2.2 the electrical field, which is present only in a grey area of width equal to d, that separates electrons from holes, leads to a potential difference (voltage)[14]. The voltage, termed the open-circuit voltage (V_{OC}), can be detected even when the junction is not linked to any external electrical circuit. Similarly, when an electrical connection is formed between the two semiconductor terminals, carriers will flow through it, moving from the n to p region.

2.1.2 Energy Storage

Due to the unpredictable and uncontrollable nature of renewable energy source (RES), the energy generated through its utilization often needs to be stored to maximize production and meet the correct energy demand in

electrical grids. For example, considering the nature of solar energy, the power gathered via PV technology is constrained by the availability of the sun. Therefore, if a typical user, such as a household, were to rely solely on PV technology, a significant portion of the generated energy would be wasted. Figure 2.3 illustrates oversimplified examples of daily energy load profiles for a typical household and PV power generation.

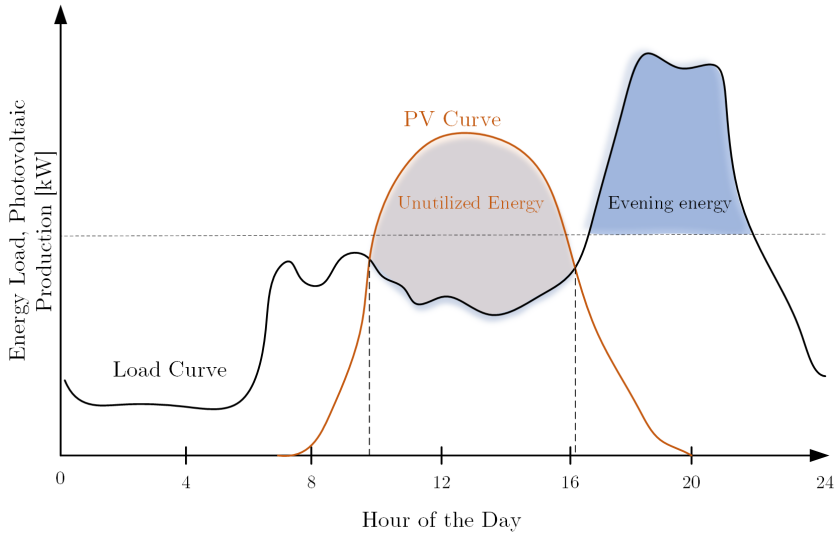

Figure 2.3: Simplified example of a typical load profile and PV generation profile [15, 16]

As observed, the power generated by the PV system is available only during the day when there is enough sunlight striking the PV panels. However, during the day, a typical household does not consume much power. Consequently, an excess of power, represented as the difference between the power generated by the PV system and the power consumed, goes unused. Nevertheless, if this excess energy were stored, it could be utilized to compensate for evening energy needs. Therefore, to store the energy and later utilize it efficiently, an energy storage system (ESS) is needed. A typical ESS accumulates energy generated with the help of RES in the form of electricity, by converting electricity to other forms of storable energy, such as chemical, thermal, potential, and hydro. When there is a necessity to withdraw the electricity, the storable energy is then converted back to electricity. Despite the development and improvement of various types of ESS worldwide, battery energy storage system (BESS) has received heightened attention in recent years due to its applicability in a wide range of situations, including power quality assurance, transmission and distribution, appliances, and voltage regulations[17]. Electric batteries serve as devices for storing electric energy in electrochemical form and supplying DC electricity[17].

2.2 Microgrids

While DER is an extremely promising group of technologies, scaling the utilization of DER up to a size, capable of satisfying the energy demands, can be challenging due to controlling issues[18]. The MG concept which was presented around 2 decades ago[7], is one of the possible solutions to efficaciously addressing this issue. A typical MG can be defined as a LV or a MV distribution system, encompassing traditional power sources, such as synchronous generators, three-phase induction generators and diesel generators, ESS, RES, power grid, loads and a controlling unit. MGs have the flexibility to operate according to the principles of either AC power systems, denoted as AC MGs, or DC power systems, referred to as DC MGs[19]. Details on DC MGs will be provided in a dedicated chapter later in this thesis. Usually, the MG is also connected to the power grid on the distribution level[20], usually to MV(e.g. 11 - 66 kV) or LV(e.g. 110 - 690 V) networks, depending on the location and the capacities of the installed units[21], to be able to meet the energy demand in case of unavailability of the MG's power generation units, or to provide electricity to the power grid it is connected to. Additionally, the MG can be functional as an independent unit without the connection to the power grid. Such operational mode is called islanding and provides the MG an opportunity to be fully functional in case of unexpected occasions, e.g. outages in the main power grid. Figure 2.4 illustrates a typical structure of the MG with the main power grid, MG substation playing a role of the controlling unit, loads represented as commercial, residential or industrial consumption, DER and point of common coupling (PCC). The PCC is a point where a transfer of power happens between the MG and the main power grid[22]. Moreover, the MG provides an improved flexibility to satisfy power quality (PQ) needs[23].

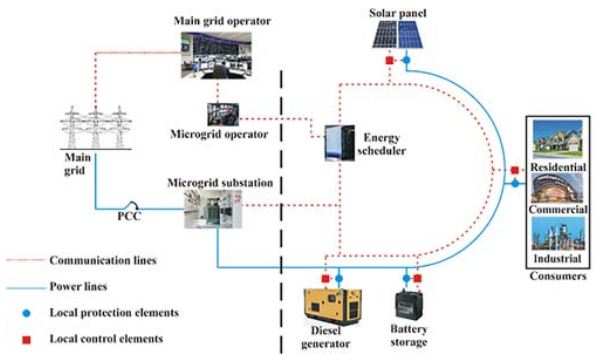

Figure 2.4: A typical structure of the MG[24].

2.3 Control of Microgrids

The primary difficulties in managing MG operations revolve around maintaining voltage and frequency control to achieve local power equilibrium,

particularly in islanding mode. Additionally, higher-level control mechanisms (depicted in Figure 2.5) aim to optimize economic benefits for the MG owner[25].

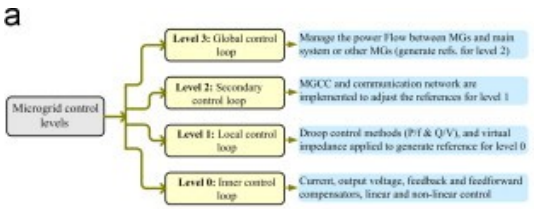

Figure 2.5: Hierarchical levels in MGs[19]

As mentioned in Sections 2.1.1 and 2.1.2, individual DER output electricity in DC form. However, in case of MGs, which facilitate an AC common interconnection(usually referred as a bus), it is needed to convert the DC electricity from the DC to AC form. In the MG this task is fulfilled by power-electronic inverters. Therefore, inverters play an important role in the MGs. Additionally, the inverters provide an interface between power generation units, loads and the main power grid[26]. Inverters are frequently connected in parallel to form power systems, either to enhance performance or achieve a higher system rating. The parallel operation of inverters also provides increased reliability compared to a single centralized source. In the event of an inverter failure, the remaining $(n-1)$ modules can still deliver the required power to the load. This enhanced reliability is further motivated by the growing utilization of RES[27]. Usually, the control of the MG is considered to be a part of decentralized approach[28] with a several different techniques presented for proper control of parallel-connected inverters, e.g. droop control[29]. Furthermore, Figure 2.5 illustrates the hierarchical levels of control in the MGs, with reference to microgrid central controller (MGCC)[19]. The following subsections 2.3.1, 2.3.2 and 2.3.3 extensively describe several control techniques for MGs, with a help of information taken from [29].

2.3.1 Conventional Droop Control

The droop control strategy is commonly implemented in synchronous generators to facilitate power sharing among multiple generators operating in parallel, ensuring their stable operation[30]. This approach, well-suited for decentralized control of parallel power sources, was initially introduced for power inverters in [31].

In the conventional droop control technique, the impedance which takes place on the output of the inverter is presumed to be entirely inductive due to highly inductive line impedance and big inductive filter[29]. The equivalent circuit diagram of two inverters, represented as a source of AC voltage, connected in parallel to a point of common coupling bus is shown in Figure 2.6 (a), and the phasor diagram is shown in Figure 2.6 (b).

Despite the fact that traditionally inverters' topologies were represented as a source of current, voltage source topology is used for high-power applica-

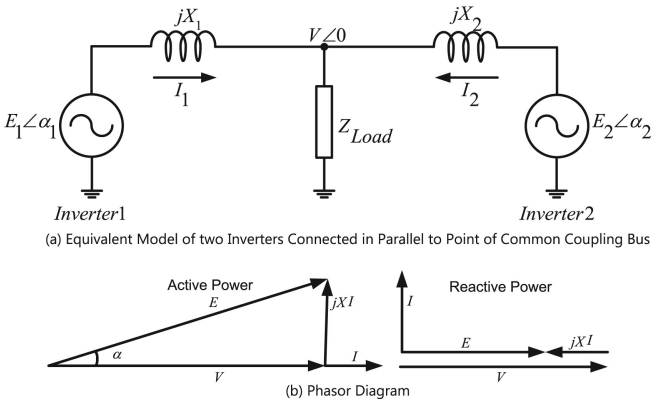

Figure 2.6: (a) Equivalent model of two inverters connected in parallel to the PCC bus[29].

tions[31]. In an inductive system, the active and reactive power drawn to the bus from each inverter can be expressed as follows[29]:

$$P = \frac{EV \sin \alpha}{X}, \tag{2.1}$$

$$Q = \frac{EV \cos \alpha - V^2}{X}, \tag{2.2}$$

where E and V are the maximum values of the inverter output voltage and the common bus voltage, respectively, α is the power angle (the phase shift between E and V), and X is the output reactance of the inverter[29]. Based on equations (2.1), (2.2) and small power angle α ($\sin \alpha \approx \alpha$ and $\cos(\alpha) = 1$), the active power injected from the inverter to the common bus is strongly influenced by the power angle. By contrast, there active power is strongly dependent on the amplitude difference between E and V. In addition, the inverter output voltage phase angle can be adjusted by changing the inverter output voltage frequency. Hence, the control of the parallel-connected inverters mainly uses the frequency droop and output voltage droop to control the output power of the inverter[29]. A block diagram of the conventional droop control is shown in Figure 2.7.

Moreover, the equations of the droop characteristics of active power - frequency ($P - \omega$) and reactive power - voltage ($Q - E$) in Figure 2.8 (a) and (b) can be written as follows[29]:

$$\omega_K = \omega^\bullet - m_K P_K, \tag{2.3}$$

$$E_K = E^\bullet - n_K Q_K, \tag{2.4}$$

where P_K, Q_K, m_K and n_K are the real active power output, real reactive power output, frequency droop coefficient, and voltage droop coefficient of the K^{th} inverter, respectively. Moreover, $\omega^\bullet$ is the rated frequency, and $E^\bullet$ is the rated voltage amplitude. The m_K and n_K are derived from equations 2.3 and 2.4, as follows[29]:

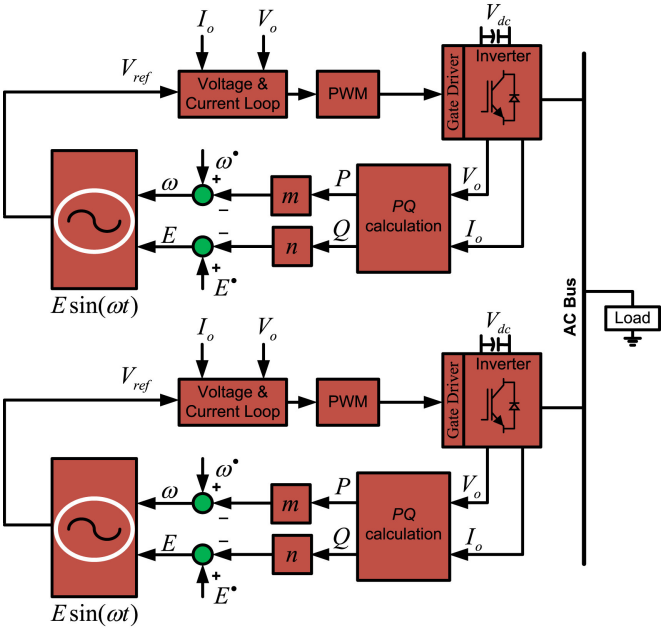

Figure 2.7: Block diagram of conventional droop control[29].

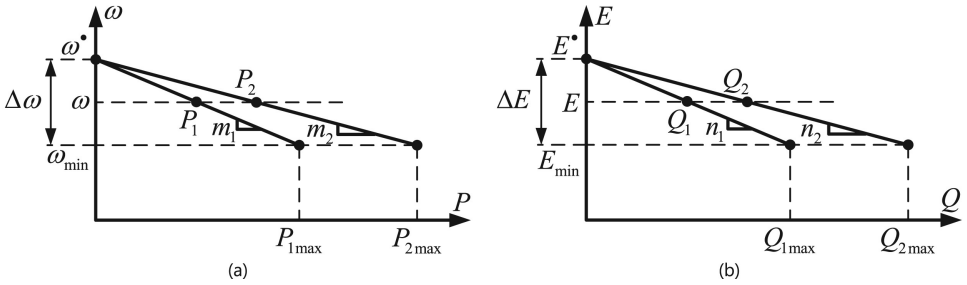

Figure 2.8: (a) $P-\omega$ and (b) $Q-E$ characteristics[29].

$$m_K = \frac{\Delta\omega}{P_{Kmax}}, \tag{2.5}$$

$$n_K = \frac{\Delta E}{Q_{Kmax}}. \tag{2.6}$$

$\Delta\omega$, ΔE, P_{Kmax} and Q_{Kmax} are the maximum allowed deviation of frequency, maximum allowed deviation of voltage, nominal active power supplied by the system and nominal reactive power supplied by the system, respectively. If the droop coefficients are increased, that increase will result in decent power sharing, but worsened voltage regulation[29]. The inherent compromise associated with this controller lies in the choice of the droop coefficient value. The primary benefit of the droop control technique is its ability to operate without relying on critical communication links between parallel-connected inverters. This lack of communication links among parallel-connected inverters offers significant flexibility and enhances reliability. However, the conventional

droop technique is not without its limitations, including a slow transient response, an inherent trade-off between voltage regulation and load sharing, bad harmonic load sharing among parallel-connected inverters when dealing with non-linear loads, line impedance mismatch affecting active and reactive power sharing, and less effective performance when integrated with renewable energy resources[29].

2.3.2 Virtual Impedance Based Droop Control

The conventional droop control method faces challenges in achieving equitable distribution of reactive power among parallel-connected inverters when there is a mismatch in line impedance. Consequently, the disparity in reactive power sharing poses a significant issue in an AC MG. Various studies have tackled this problem by incorporating virtual output impedance into the droop control approach through a rapid control loop that simulates the line impedance (see Figure 2.9)[29].

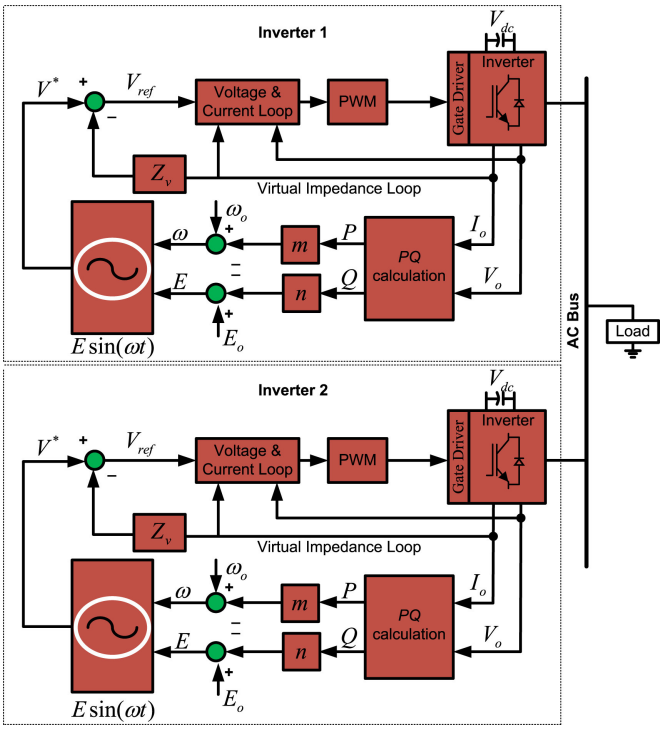

Figure 2.9: Virtual impedance loop-based droop control[29].

This modification allows for the adjustment of the reference voltage from each inverter, as outlined by Tayab et al.[29].

$$V_{ref} = V_O^* - Z_v I_O. \tag{2.7}$$

Z_v denotes the virtual output impedance. Figure 2.10 illustrates the equivalent model of virtual impedance and the phasor diagram for the scenario where $Z_v > Z_l$, as depicted in parts (a) and (b), respectively.

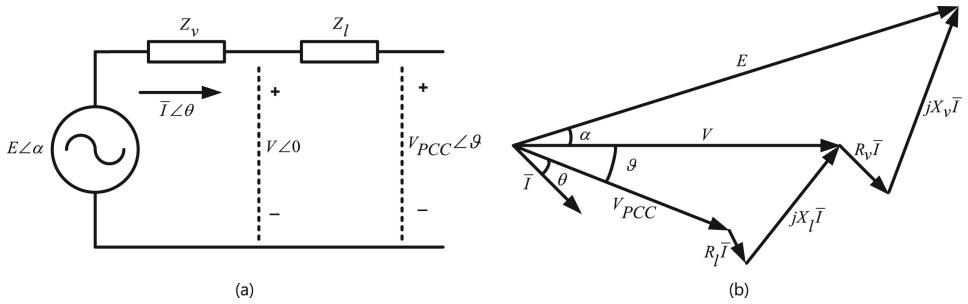

Figure 2.10: (a) Equivalent model of a virtual impedance and (b) Phasor diagram[29].

The virtual output impedance is typically chosen to dominate the line impedance[29]. This selection is often achieved through the summation approach, wherein balanced reactive power sharing is attained by ensuring the voltage drop from each inverter to the AC bus follows the relationship[29]:

$$V_{drop1} = (Z_{l1} + Z_{v1})I_{l1} = V_{drop2} = (Z_{l2} + Z_{v2})I_{l2}, \tag{2.8}$$

Z_{v1} and Z_{v2} represent the virtual output impedance of two parallel-connected inverters, while Z_{l1} and Z_{l2} denote the line impedance of the corresponding inverters. In the summation approach, one virtual output impedance is set to zero, and the other is configured to mimic the line impedance. With consideration for equation (2.8) and the assumption that one line impedance is greater than the other, i.e., $Z_{l1} > Z_{l2}$, allowing for the selection of $Z_{v1} = 0$, equation (2.8) can be simplified as[29]:

$$Z_{v2} = Z_{l1} - Z_{l2}, \tag{2.9}$$

The application of the summation approach reduces the value of the virtual impedance, minimizing the impact on voltage regulation. Enhanced reactive power sharing is achieved when the change in output voltage significantly surpasses the voltage drop across the line in comparison to the reactive power[29].

2.3.3 Adaptive Droop Control

The conventional droop control encounters various challenges, including line impedance dependency, imprecise power sharing, and a sluggish transient response[29]. Consequently, alternative forms of droop control have been proposed to tackle these issues. In 2002, Kim et al. introduced the adaptive droop control strategy, aiming to maintain voltage amplitude significantly while ensuring accurate reactive power sharing[29, 32]. In this approach, the maximum reactive power Q_{max} drawn from each unit is stored and compared with the reference value of reactive power Q_{ref}. If the maximum reactive power is less than the reference value, the voltage amplitude follows the

traditional $Q - E$ droop equation. However, if the maximum reactive power exceeds the reference value, the voltage amplitude is determined as follows[29]:

$$E = E^* - nQ - n_{add}(Q - Q_{ref}). \tag{2.10}$$

Hence, $Q > Q_{ref}$. The fundamental concept of adaptive droop control is depicted in Figure 2.11.

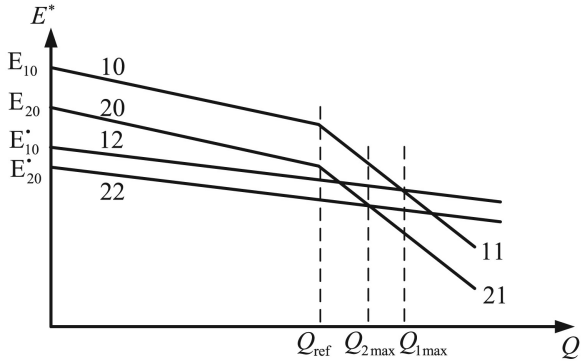

Figure 2.11: Basic concept of adaptive droop control[29].

The difference between the output reactive power Q and the reference value of reactive power Q_{ref} is utilized as an additional value to establish the desired voltage amplitude. When $Q > Q_{ref}$, the voltage amplitude transitions from lines 10 and 20 to lines 11 and 21. The maximum reactive power is stored, and $n_{add}(Q_{max} - Q_{ref})$ is subtracted from the voltage amplitude as a constant value. Consequently, if Q decreases below Q_{ref} again, the voltage amplitude does not revert to lines 10 and 20 but to lines 12 and 22. This phenomenon is expressed in equation (2.11).

$$E = E^* - nQ - n_{add}(Q_{max} - Q_{ref}), \tag{2.11}$$

2.4 DC Microgrids

The other type of existent MGs is the one based on DC power. The reasons and purposes for utilizing such kind of MGs were greatly described by Justo et. al in [19] and in this paragraph it is summarized. The traditional electric power system was initially devised to transmit central station AC power through high-voltage AC transmission lines and lower voltage distribution lines to households and businesses employing the power in devices like incandescent lights, AC motors, and other AC equipment. Conversely, DC power systems found application in industrial power distribution, telecommunication infrastructures, and point-to-point transmissions over extended distances or through sea cables, as well as in interconnecting AC grids with varying frequencies. Present-day consumer equipment and future DER units heavily rely

on power electronics devices. These devices, including computers, fluorescent lights, variable-speed drives, households, businesses, and industrial appliances, operate on DC power. However, most of these DC devices necessitate the conversion of available AC power into DC for their usage, and the predominant portion of these conversion stages commonly involves inefficient rectifiers. Additionally, power from DC-based DER units must undergo conversion into AC to integrate with existing AC electric networks, only to be reconverted into DC for many end users. These consecutive DC–AC–DC power conversion stages result in significant energy losses. Capitalizing on positive experiences in high voltage direct current (HVDC) operation and advancements in power electronics technology, there is a growing interest in the pursuit of effective solutions. The low voltage direct current (LVDC) distribution network emerges as a novel concept and a potential solution to current power distribution challenges, envisioning the future power system. It incorporates features aligning with the new requirements of electrical distribution networks. Figure 2.12 illustrates typical DC MG systems interconnected with main systems at the PCC, which could be a medium voltage AC (medium voltage alternating current (MVAC)) network from conventional power plants or an HVDC transmission line linking an offshore wind farm[19].

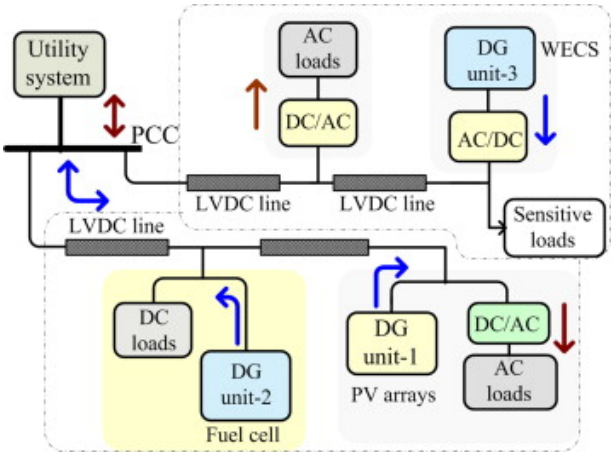

Figure 2.12: Concept of a DC MG system with the DER units and mixed types of loads[19].

2.4.1 Control of DC MGs

Several control strategies utilized in DC MGs have a lot in common with the control strategies used in AC MGs. One example of a commonly used strategy[33, 34] in DC MGs is droop control. This strategy utilizes slightly modified droop characteristics as shown in the equations as follows[34]:

$$V_{DCK} = V_{DC} - m_{cp}P_{oK}, \tag{2.12}$$

$$V_{DCK} = V_{DC} - m_{cc}I_{oK}, \tag{2.13}$$

where V_{DCK}, V_{DC}, m_{cp}, m_{cc}, P_{oK} and I_{oK} are reference voltage of the K^{th} converter, bus voltage, power droop coefficient, current droop coefficient, output power of the K^{th} converter and output current of K^{th} converter, respectively. Illustration depicting the principles of droop for power and current, respectively, are presented in Figure 2.13.

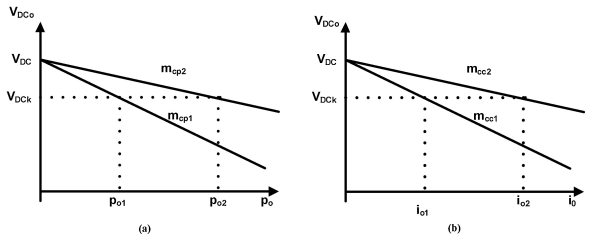

Figure 2.13: Power Droop Curves (a) and Current Droop Curves (b)[34].

The system's current sharing, accuracy, and stability are influenced by the values of the droop coefficients. A higher droop coefficient leads to a more damped system, enhancing accuracy in current sharing while simultaneously increasing voltage deviation. Therefore, a necessary trade-off exists between current sharing, accuracy, and voltage deviation[34]. In DC MGs, the interface between DERs and the MG is commonly referred to as a converter, in contrast to inverters as discussed in Section 2.3.

2.5 Motivation

In the prior sections, an overview of MGs and their applications was provided. Subsequently, various control strategies were detailed. Recognizing that nearly every control strategy involves calculations related to voltages, currents, or powers, the goal of this bachelor thesis is to enhance the overall stability of DC MGs by implementing stabilization and algorithmic filtering for these crucial measurements. The motivation for this initiative arises not only from the inherent complexity of control strategies but also from the desire to mitigate potential instabilities and improve the performance of DC MG systems. Furthermore, during a comprehensive review of pertinent publications addressing stability issues in MGs, it was observed that many of them leverage voltage and other measurements[8, 9, 35]. Therefore, the filtering and stabilization methods are not only pertinent to the specific context of DC MGs but may also find application in addressing stability challenges across various types of MGs.

Chapter 3

Technical Resolution

For the technical part of this study, i.e. parameters improvement, it is necessary to describe the DC microgrid (DC MG) that will be examined. The specifications of the devices that are incorporated in this DC MG will be provided, as well as an energy balance of the DC MG, to explore the energy flow and usage in the current state. Additionally, before implementing a solution in the examined DC MG, it is needed to validate the solution via the simulation software called Simulink. Hence, the simulation overview will be presented in this chapter. At the end, the solution that will be implemented in the examined DC MG will be overviewed and the outcomes of this solution will be presented.

3.1 Examined DCMG

A DC MG to be examined in this thesis adopts common configuration, comprising one energy storage, a PV generation array, multiple loads, and a PCC. This DC MG follows a topology commonly known as radial or single bus topology[36]. The single bus of the examined DC MG has a nominal voltage equal to $700V$. Figure 3.1 illustrates the topology of the examined DC MG.

The table 3.1 gives detailed overview on the devices used in the examined DC MG.

Block	Device	Manufacturer / Model	Rated Power/Capacity
T	Transformer	Elektrokov TOC 3100100	40 kVA
C1	AC/DC Converter	Zekalabs LB 1095	25 kW
C2	DC/DC Converter	Zekalabs LB-1071-04-01	40 kW
C3	DC/DC Converter	Zekalabs LB-1071-04-01	40 kW
EV1	DC/DC Converter	Zekalabs LB 1132	25 kW
EV2	DC/DC Converter	Zekalabs LB 1132	25 kW
A	Active Front-End	Delta AFE 2000	37 kW
EMU	DC Load Emulator (Heat Pump)	InterPro ELR 9000 HP	15 kW
Battery	BESS	Eaton xStorage	50 kWh
PV	Array of PV panels	Jinko JKM270PP-60-V	17 kWp
MGCC	Microgrid's Controller	Eaton SMP SG-4260	-

Table 3.1: Devices' specifications

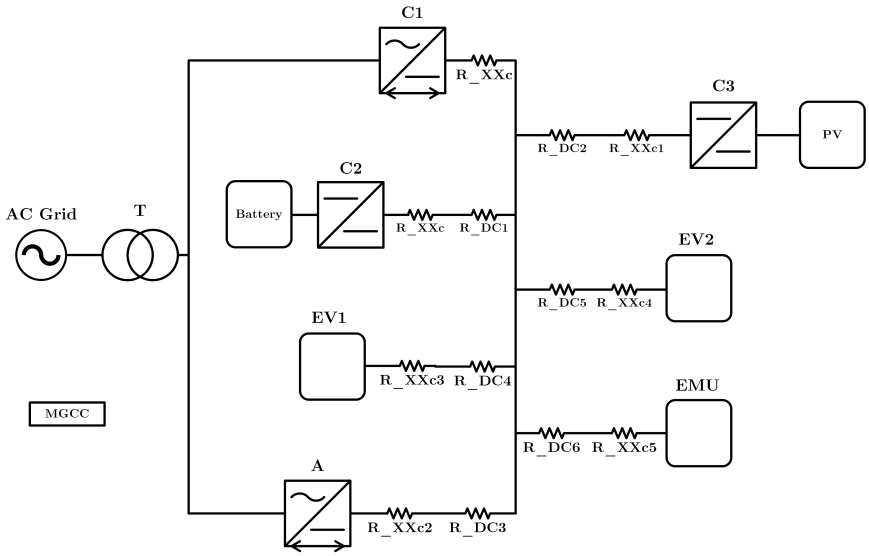

Figure 3.1: Topology of the examined DC MG.

In this DC MG $C1$ and A can function as grid-forming sources[37], however in this thesis only $C1$ will be utilized as a grid-forming device. Consequently, all other DC MG's devices will be grid-following. The blocks $EV1$ and $EV2$ are used as load emulators for electric vehicle (EV) chargers. The block EMU is used as a DC load emulator for a heat pump. Additionally, from the Figure 3.1 it can be seen that another prevalent issue within DC MGs is the occurrence of voltage drops across the common bus, which can be attributed to line impedance. These voltage drops hinder distributed energy resources from employing power-sharing strategies in the most efficient manner.

3.2 Energy Balance

The MGCC of the the examined DC MG has a feature which allows to log specific measurements into the database. The data then can be gathered from the database using the Matlab scripts. Such organization provides an opportunity to explore the profiles and measurements in the different time ranges. However, at the moment the examined DC MG has an opportunity to measure and log the power consumption data only for one part of the whole building. Meaning, that the power consumption data that will be provided later in the thesis will be less than the actual one for the whole commercial building. For instance, power profiles from 16th June 2023 to 20th June 2023 were collected and shown on the Figure 3.2, where the red, green, yellow and blue profiles on the top graph represent power flow in or out of the DC MG, power flow in or out of the BESS, the building's consumption and the PV generation profile, respectively. During this time period the BESS was only connected to the DC-bus, but was not used for charging or discharging due to the development process which required no power flow from or to the battery.

The theoretical possibility to compensate part of the daily consumption via the PV and the BESS will be explored later in this subsection.

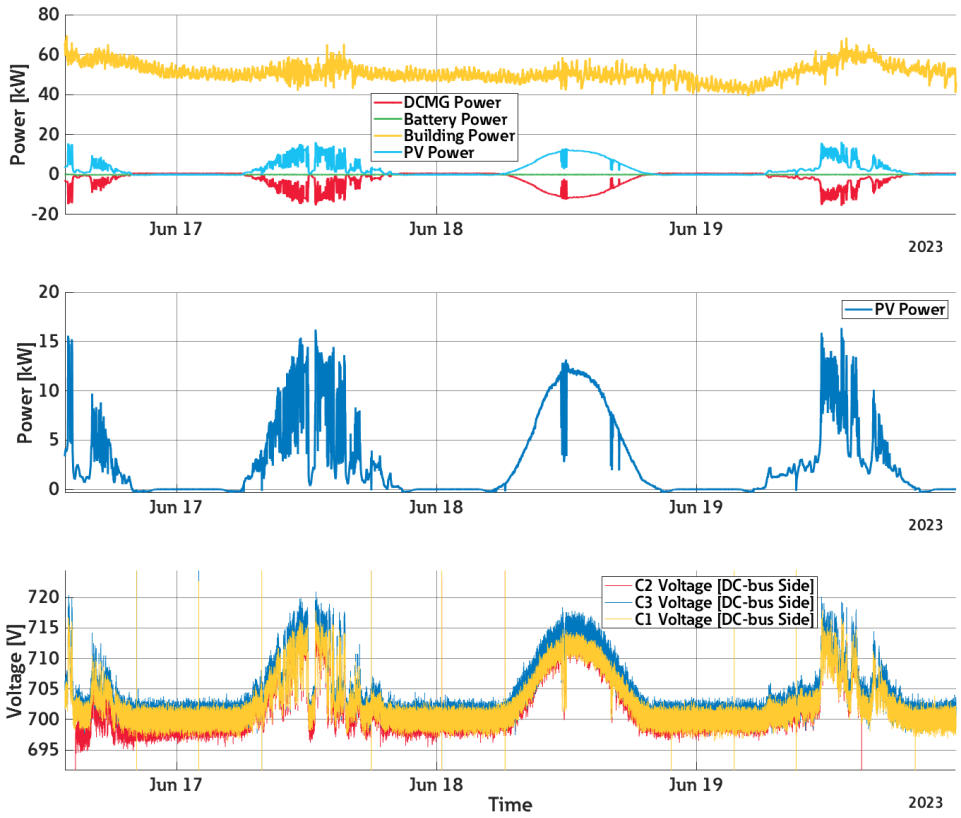

Figure 3.2: Energy consumption profile of the building and PV generation profile, from 16th June to 20th June.

Additionally, the data for energy can be gathered for individual months and is presented in the Table 3.2, where P_{Avrg}, E_{TotB}, E_{TotPV}, d and ΔE are average power consumed by the building, total energy consumed by the building, total energy generated via PV, a ratio of total energy generated via PV to total energy consumed by the building respectively and an absolute value of difference between average of total energy consumed by the building and total energy consumed by the building for individual month, respectively.

It can be seen that the highest deviation from the average value for energy consumption occured on August 2023. Since, the examined DC MG is placed in the research & development (R&D) center, the building consumption can vary based on the power electronics technologies being tested during specific occasions, meaning an increase of power consumption during those tests. Moreover, the acquired data of the energy generated via the PV can be compared to the data received via a tool by european commission[38]. The comparison can be seen from the Table 3.3, where d_{real}, E_m and T_{Loss} are ratio of measured energy generated by the PV to total energy consumed by the building, theoretical average monthly energy production by the PV and a difference between theoretical average monthly energy production by the

Month	P_{Avrg} [kW]	E_{TotB} [MWh]	E_{TotPV} [MWh]	d [%]	ΔE [MWh]	ΔE [%]
November-22	48.51	34.88	0.18	0.52	3.24	8.5
December-22	51.69	38.38	0.06	0.16	0.26	0.7
January-23	54.88	40.50	0.13	0.32	2.38	6.3
February-23	51.5	34.58	0.26	0.75	3.54	9.3
March-23	51.45	38.25	0.7	1.83	0.13	0.4
April-23	49.51	35.59	1.34	3.77	2.53	6.6
May-23	52.36	38.91	1.93	4.96	0.79	2.1
June-23	51.23	36.92	2.43	6.58	1.20	3.1
July-23	50.57	37.91	0.75	1.98	0.21	0.5
August-23	54.63	43.50	1.04	2.39	5.38	14.1
September-23	52.26	39.74	0.21	0.53	1.62	4.3
October-23	53.19	38.23	0.76	1.99	0.11	0.3
Total		457.39	9.79	2.14		
Average	51.82	38.12	0.82	2.13		

Table 3.2: Monthly data acquired via MGCC.

PV and measured energy generated by the PV.

Month	E_{TotB} [MWh]	E_{TotPV} [MWh]	d_{real} [%]	E_m [MWh]	T_{Loss} [MWh]
January	40.5	0.13	0.32	0.70	0.57
February	34.58	0.26	0.75	1.02	0.76
March	38.25	0.7	1.83	1.59	0.89
April	35.59	1.34	3.77	2.14	0.80
May	38.91	1.93	4.96	2.20	0.27
June	36.92	2.43	6.58	2.21	-0.22
July	37.91	0.75	1.98	2.23	1.48
August	43.5	1.04	2.39	2.09	1.05
September	39.74	0.21	0.53	1.79	1.58
October	38.23	0.76	1.99	1.26	0.50
November	34.88	0.18	0.52	0.70	0.52
December	38.38	0.06	0.16	0.62	0.56

Table 3.3: Comparison between measured data and expected data gathered from [38].

From the comparison table it can be seen, that for almost all months there is a significant amount of energy that is not generated. Such loss can be explained with the fact, that the examined DC MG is still under development and during the development process it may and it happened that some of the devices or control algorithms do not work properly or as expected. For instance, in July and August the power production is extremely low, even though the expected generated energy is much more. This loss happened due to the breakage of the converter $C3$, which happened due to the wrongly implemented control algorithms.

Moreover, the energy balance of the DC MG for one day will be explored. Since the building's consumption profile is almost similar during the whole year with exceptional spikes during short tests, the day on 29th June was chosen for the analysis. Figure 3.3 illustrates the profiles of building for the specified day.

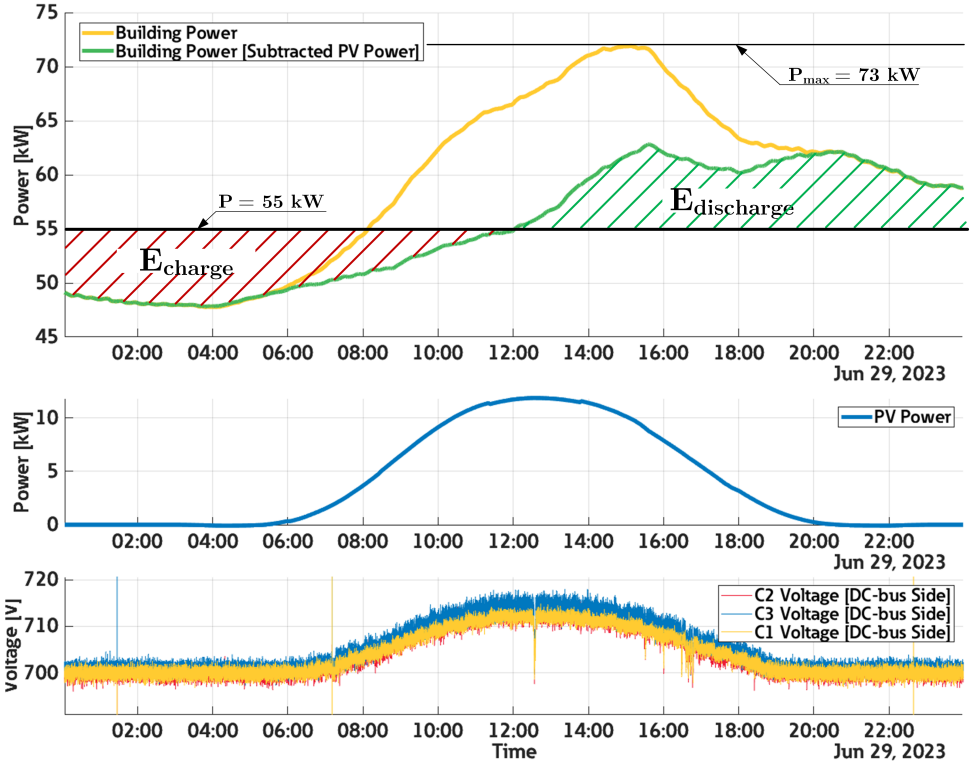

Figure 3.3: Energy balance of the examined DC MG on 29th June.

From the Figure 3.3 it can be seen that the consumption slightly increases during the working hours, when employees are in the building. The profile named "Building Power [Subrtacted PV Power]" represents a power profile after compensation the consumption with the PV by subtracting the value of the PV power from the building power value. The energy $E_{discharge}$ in green is the building's energy that is compensated with a help of the BESS by discharging the battery system. The energy used to charge the BESS, i.e. E_{charge}, is highlighted with red area. In that case, it can be derived, that on this day, the BESS with a capacity 50 kWh could be charged and then fully compensate the E_{charge} with the help of the energy generated via the PV. Additionally, such compensations are useful in cases of limited reserved capacity arranged with an energy distributor. For instance, if the contract between the building's owner and the energy distributor had reserved capacity set at 60 kW, the building's owner would pay extra for exceeding the reserved capacity.

3.3 Parameters Improvement

This section will provide crucial details about the simulation project, where the examined DC MG will be modeled. Additionally, technical solutions for parameters' improvement will be implemented in the simulation for validation

and the overview will be presented.

3.3.1 Simulation

For easier development process a simulation software called Simulink will be used. Simulink serves as a block diagram environment designed for multidomain simulation and Model-Based Design. A simplified electrical diagram of the DC MG implemented in Simulink is presented in Figure 3.4.

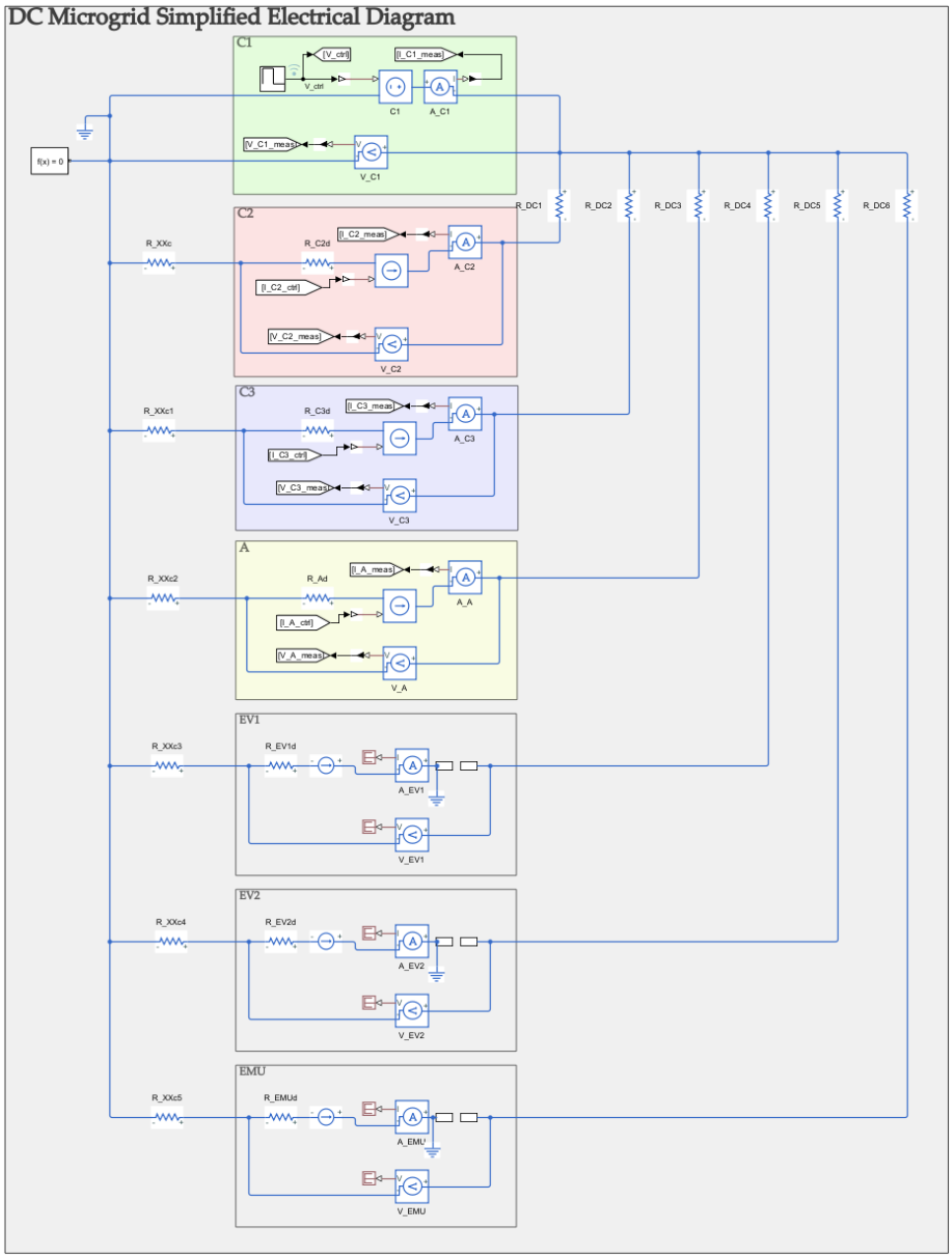

Figure 3.4: Simplified electrical diagram of the examined DC MG in the simulation.

Given that all connected devices have isolated inputs and outputs, only parts of the converters linked to the shared DC bus are included in the electrical diagram. The output capacitance of power converters is neglected. Additionally, emulators EV1, EV2 and EMU are "turned-off"(open-circuit), since in this study their functionality may be neglected and they are included to increase the number of nodes where voltage drop can occur. Internal resistances of the power converters are denoted with a letter d and all are estimated to be $20\,\Omega$, because those resistances are used to adjust voltage across device's terminals, using controllable current source, that sets a current, which in combination with internal resistance will create a voltage equal to the DC-bus voltage. For instance:

$$V_{DC-bus} = I_{C2} \cdot R\_C2d = 700\,V \tag{3.1}$$

Resistances R_XXc_i represent the resistance of the cables which connect the device to the DC-bus. The approximation of cables' resistances will be performed under the following assumptions:

- The cable material used for all connections is copper,
- The resistivity of the cable: $\rho = 1.72 \cdot 10^{-8}\ \Omega \cdot m$,
- Nominal voltage: $V_{nom} = 700\,V$,
- Cable cross-section area: $A_{crs} = 26.6705 \cdot 10^{-6}\ m^2$,
- The length of all cables which connect devices to the DC-Bus: $L_{cable} = 2$ m.

Under the described assumptions cables' resistances can be approximated using the following formula:

$$R\_DC_i = 2 \cdot \frac{\rho \cdot L_i}{A_{crs}} \tag{3.2}$$

The result approximations can be found in Table 3.4, where L_i is the length of the cable from C1 to the specified device i.

	i	L_i [m]	R_DC_i [Ω]	R_XXc_i [Ω]
Battery	1	10	0,013	0,0026
PV	2	150	0,1935	0,0026
A	3	5	0,006	0,0026
EV1	4	20	0,026	0,0026
EV2	5	20	0,026	0,0026
EMU	6	30	0,039	0,0026

Table 3.4: Approximated Resistances

The noise power for the measurements was selected to be $0,01$. The reference voltage profile for the simulation was manually created via the

```
function [C2_Voltage_Compens, C3_Voltage_Compens, ...
A_Voltage_Compens] = voltageCompensation(C2_Voltage,...
C3_Voltage, A_Voltage, C2_Current, C3_Current, A_Current,...
R_XXc, R_DC1, R_DC2, R_DC3)

C2_Voltage_Compens = C2_Voltage+C2_Current*(R_DC1+R_XXc);

C3_Voltage_Compens = C3_Voltage+C3_Current*(R_DC2+R_XXc);

A_Voltage_Compens = A_Voltage+A_Current*(R_DC3+R_XXc);
```

Code 3.1: Code for voltage drop compensation in the simulation

"Repeating Sequence Stair"-block with the inspiration taken from the examined DC MG. The comparison between simulation measurements and real measurements acquired via the MGCC can be seen in Figure 3.5 *A*) and *B*).

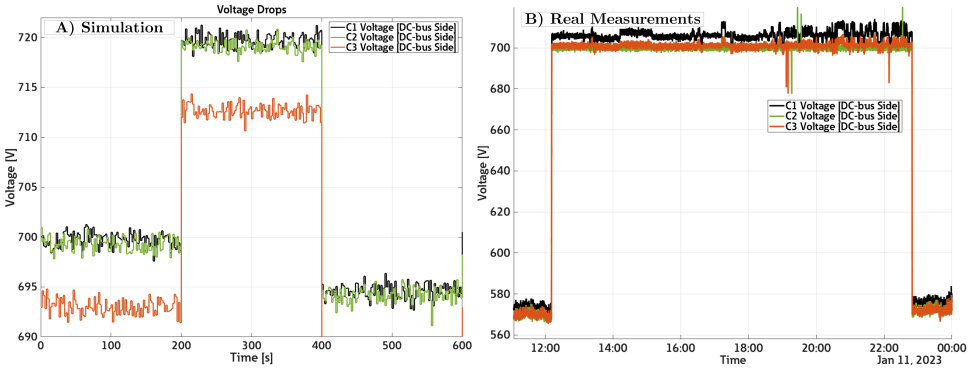

Figure 3.5: Voltage measurements profiles in the *A*)simulation and *B*)real.

From the figure it can be seen that the values of voltages differ in simulation and in the real measurements. However, values of voltages are inside of the working ranges of the specified converters. Hence, it was estimated that the effect of this difference in values is neglectable. The situation could have changed in case of values being near the limits of the specified converters.

3.3.2 Voltage Drop Compensation

The idea behind voltage drop compensation is to determine the value of the voltage drop and to set an offset for the measurements that will be the same amount as the voltage drop. In the simulation, which was described in the section 3.3.1, the compensation is implemented with the utilization of the "MATLAB Function Block", as depicted on the Figure 3.6.

The code inside of this block evaluates the resistance of the specified lines and based on the current calculates the voltage drop, as in Code 3.1.

For better visibility of the results, the noise power was reduced to 0 in the simulation. The result of such compensation can be seen on the Figure 3.7.

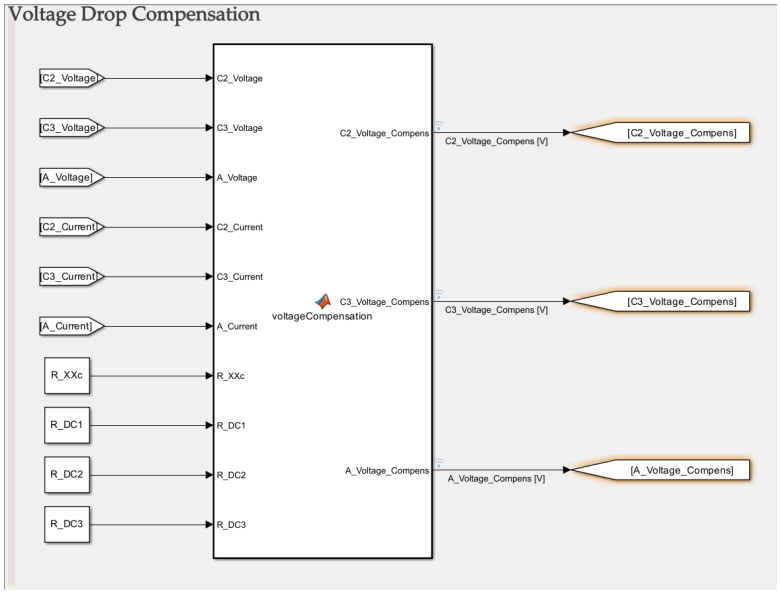

Figure 3.6: MATLAB Function Block for voltage drop compensation.

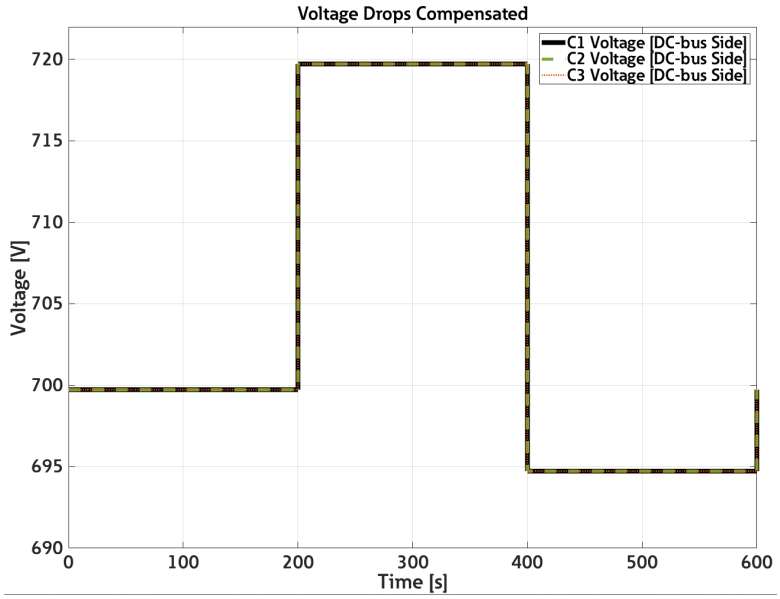

Figure 3.7: Compensated measurements in the simulation.

As it can be seen, the voltages across devices' terminals are equal to the voltage of the grid-forming device $C1$. However, it is needed to be aware, that te simulation was modeled under specific assumptions and almost ideal circumstances, meaning that the real-life results might differ, based on other factors.

3.3.3 Measurement filtering

Filtering of the measurements is needed to reduce the noise coalesced with the measurements and to provide stable values for the control algorithms of the DC MG. All the measured values which are received by the MGCC are discrete-time, meaning that the values of the signal are available only at discrete intervals[39]. In this study the finite impulse response (FIR) digital filter will be implemented, due to the fact that it is one of the most common digital filters, its potential noise reduction is estimated to be sufficient for this thesis and the Simulink's additional "PLC Coder" package has an ability to generate a PLC code of the FIR filter for the MGCC.

The following definition of the common FIR filter is well described by the [39] and will be used in this section. *The causal FIR filter is characterized by a difference equation that is a linear combination of past and present input samples x(n) multiplied by the coefficients h(n). For example, the difference equation of a second-order filter is:*

$$y(n) = h(0)x(n) + h(1)x(n-1) + h(2)x(n-2). \tag{3.3}$$

Samples $\{x(n), x(n-1), x(n-2)\}$ *are the present and the past two input samples and* $\{h(0), h(1), h(2)\}$ *are the respective filter coefficients. The output is y(n). The filter length* M *is 3, which is the number of terms of the impulse response. The order* N *of a FIR filter is the filter length minus one* $(N = M - 1)$[39].

The simulation's parameters, such as simulation time, sampling time and noise power, were slightly modified to get the simulation as close as possible to the real-life DC MG. Hence, the simulation time was chosen to be 10 minutes, sampling time to be 5 seconds, because the measurements in the MGCC have this same sampling time, noise power is equal to 1 and the reference voltage profile was slighly modified. For proper function of the filter it is needed to choose appropriate filter order and coefficients. The coefficients in this thesis are found by utilization of $firceqrip$ function in Matlab as following:

```
eqnum = firceqrip(N,Fp/(Fs/2),[Rp Rst],'passedge');
```

where $eqnum$, N, Fp, Fs, Rp and Rst are vector of coefficients, filter order, passband-edge frequency, sampling frequency, maximum deviation for passband ripple and maximum deviation for stopband ripple, respectively. The discrete FIR filter in this simulation is implemented via the "Discrete FIR Filter" block, provided by the Simulink "DSP System Toolbox". After a huge amount of experimental trials it was found that the following values for $firceqrip$ function's parameters fit well for the purpose of this thesis: $\{N = 24, Fp = 0.0001, Fs = 0.5, Rp = 0.00057565, Rst = 0.0001\}$. The results of the filtering with those coefficients is shown on the Figure 3.8.

As it can be seen from the figure, the filter does filter the signal, however requires time to adjust to rapid changes. Hence, it was needed to modify the filter so that the filter can react on the rapid changes. The modification was made with a "MATLAB Function" block as depicted on the Figure 3.9

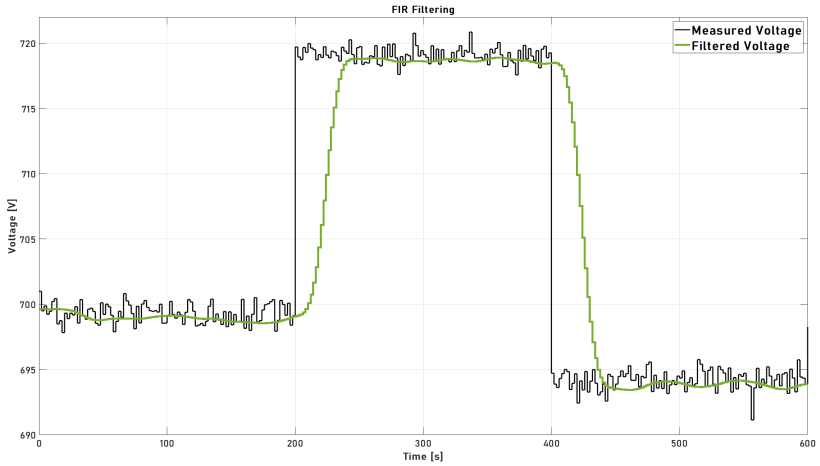

Figure 3.8: The result of FIR filtering for voltage measurements of the battery converter $C2$.

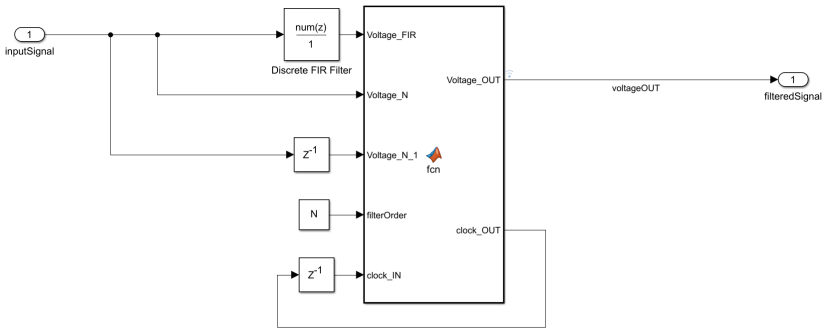

Figure 3.9: The modification of the FIR filter.

The code inside of this block is displayed in the Code 3.2.

Such modification allows the filter to quickly react on the rapid changes by sacrificing the filter efficiency at the moment of the change. Additionally, the downside of such modification is a hardcoded value of the rapid change, which in that case equals to 5. The result of the modified filtering can be seen on the Figure 3.10.

3.4 Real-Life Testing

This section will provide a thorough overview of the solutions derived from the simulation and how it was implemented in the MGCC of the examined DC MG.

3.4.1 Voltage Drop Compensation

An additional feature that the MGCC possesses is an ability to monitor measurements and control devices via the human machine interface (HMI).

```
function [Voltage_OUT, clock_OUT] = fcn(Voltage_FIR,
Voltage_N, Voltage_N_1, filterOrder, clock_IN)

if abs(Voltage_N - Voltage_N_1) > 5
    clock_OUT = filterOrder;
else
    clock_OUT = clock_IN - 1;
end

if clock_OUT > 0
    Voltage_OUT = Voltage_N;
else
    Voltage_OUT = Voltage_FIR;
end
```

Code 3.2: Code inside of the "MATLAB Function" block

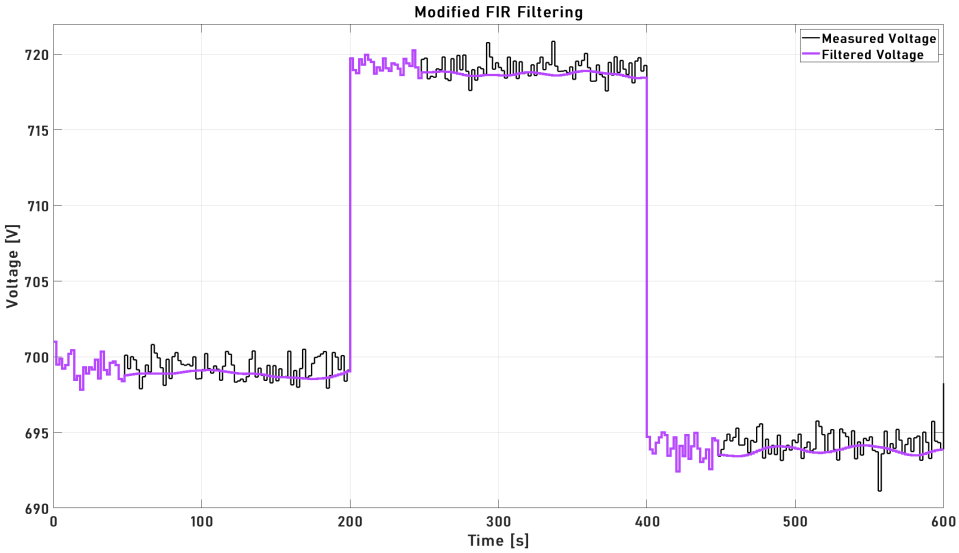

Figure 3.10: The result of the modified FIR filtering for voltage measurements of the battery converter $C2$.

For the purposes of the real-life testing the special HMI was created and illustrated on the Figure 3.11.

The top left part of this HMI allows a DC MG operator to enter the parameters for the voltage drop evaluations, such as cables' resistivity, cables' lengths and cross-section area. The code for the voltage compensation on the MGCC has the same logic as in the simulation, however is implemented in another environment called CoDeSys and specific variables needed to be renamed due to the already implemented features in the examined DC MG, as in Code E.1. The outcome of such compensation can be seen on the graph on the Figure 3.11. All the values are approaching the reference value,

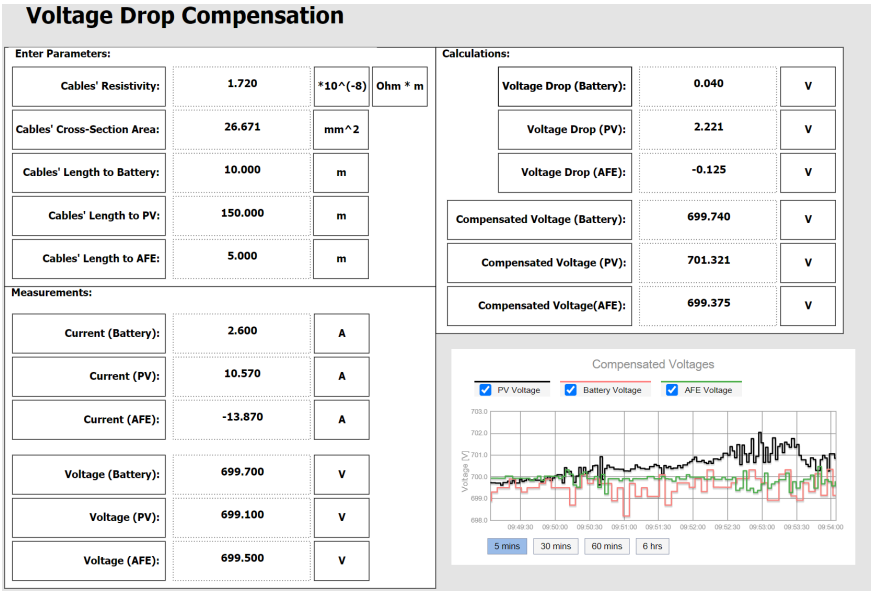

Figure 3.11: The designed HMI on the MGCC.

however in case of the PV spikes happen due to the converter's properties in combination with changing solar irradiation.

3.4.2 Measurement filtering

With the help of the simulation and the "PLC-Coder" package it was possible to generate a code for FIR filtering function block for the MGCC.

Figure 3.12: The graph of the measured and filtered voltages on the DC-bus side of the converters.

The resultant function block can be seen in the Code E.2. Additionally, it was needed to implement filtering in specific way with the use of delay to match sampling time of the filter. However, the delay functionality is not accesible directly in the CoDeSys, so it was neccessary to implement it via

the utilization of the timer function block, provided by the standart library. The implementation is provided by [40] and is displayed in Code E.3. For the purposes of this real-life testing, the graph of filtered measurements was added to the HMI and is displayed on the Figure 3.12. The outcome of such filtering is almost identical to the outcomes of the simulation results. However, multiple occurrences arose. Firstly, for all the measurements the filter was creating an offset, resulting in shifted profiles. This is most probably caused by the impulse response of the filter. Secondly, upon author's opinion it is considered that perfect filtration of measurements was not achieved due to low sampling period of the measurements, which greatly affects the effectivity of the filter. This could be achieved with an increased sampling period in the converter. Additionally, perfect filtration could be achieved with the proper adjustment of the coefficients.

Chapter 4

Economic Analysis

This chapter is aimed at evaluating economic effects of the implementation of a new theoretical control technique in the examined DC MG, which was also partially described in the section 3.2. This technique involves building's power compensation based on the available energy generated via the PV and energy stored in the BESS, to lower expenses associated with energy consumption. For better results, it is also needed to provide more detailed specifications of the devices inolved in this study, such as battery packs and solar cells. Additionally, it is needed to provide an information about the current building's tarif.

There are 64 solar panels installed on the roof of the building, facing North. Individual panel's model is Jinko JKM270P-60[41]. Moreover, the examined DC MG provides an opportunity to change solar panels' configuration, based on the requirements. For instance, the panels can be either connected in two parallel branches of 32 panels connected in series, or in 4 parallel branches of 16 panels connected in series, based on the requirements. The maximum power that can be provided by this PV electric plant is 17 kWp.

The BESS consists of five battery packs xStorage Compact GEN4[42] connected in series. The maximum amount of energy which can be stored in this BESS is 50 kWh.

The building's tarif is displayed in the Table 4.1.

Accounted total amounts - breakdown of electricity supply and regulated services		
Item	Unit	CZK/Unit
Power Electricity	MWh	3 470,00
Electricty Tax	MWh	28,30
Grid Usage	MWh	117,39
Unsolicited supply of reactive energy	MVArh	440,00
Reserved capacity (month)	MW	224 120,00
Reserved capacity (year)	MW	202 480,00
Market's operator activity	month	4,14
Support of electricity from supported sources of energy	MWh	495,00
System's services	MWh	212,82
VAT rate	%	21

Table 4.1: Building's electricity tariff breakdown.

In this table electricity tax means a taxation according to part 47. Act No. 261/2007 Coll. the law on the stabilization of public budgets. According to this law, the final customer is obliged to declare and pay the tax. Exceptions are cases where the supplied electricity is exempt from this tax. Moreover, later in the text, the electricity trade will appear in the breakdown tables. The electricity trade shows the sum of the costs associated with the supply of electricity from the electricity distributor, that is, the sum of the price of power electricity and the electricity tax.

4.1 Economic Methods

For a proper economic analysis it is needed to define a method which will be used for the evaluation. Methods such as net present value (NPV), internal rate of return (IRR) and equivalent annual cost (EAC) will be briefly described and a combination of those will be then utilized for the analysis.

4.1.1 Net Present Value

Net Present Value is one of the methods for economic analysis of investments. It is a method of evaluating the expected outcome of the investment by translating the future value of the money, into today's value, while also considering the riskiness of the investment, through the discount rate r. The value of NPV can be found as following[43]:

$$NPV = C_0 + \sum_{t=1}^{T} \frac{C_t}{(1+r)^t}, \tag{4.1}$$

where C_0, T and C_t are value of investment represented as a negative number, economic life of the investment and the cash flow in the associated year t, respectively. To determine whether the investment is worth pursuing, a citation from [43] can be used: *net present value is the addition that the investment makes to your wealth.* That means, that the bigger the value of the NPV, the bigger return will the investment bring.

Additionally, other advantages of NPV can be provided[43]:

- NPV offers clear benchmark for comparing projects. Projects with negative value of NPV should not be taken into the consideration, while projects with positive value should be accepted.
- NPV depends on good cash flow forecasts in the project. Any rule which ignores specific cash flows will lead to poor financial decisions.
- NPV acknowledges that *a dollar today worth more than a dollar tomorrow.*
- NPV is dependendent solely on the forecasted cash flows and the opportunity cost of capital. It is not affected by the profitability of the company's

existing business, or the profitability of other independent projects. Nor is it affected by the company's choice of accounting method.

- If you have two dollars in your purse and one dollar in your pocket, you own in total three dollars. That is obvious. Similarly, because present values are all measured in today's dollars, you can add them up. Therefore, if you have two projects A and B, the net present value of the combined investment is:

$$NPV(A+B) = NPV(A) + NPV(B). \tag{4.2}$$

4.1.2 Internal Rate of Return

The IRR is a close relative of NPV and is capable of providing the same result if used appropriatly. The IRR is a such discount rate, when the NPV equals zero, i.e.[43]:

$$NPV = C_0 + \sum_{t=1}^{T} \frac{C_t}{(1+IRR)^t} = 0. \tag{4.3}$$

Additionally, NPV values implied by a range of discount rates can be plotted to better visualize the IRR, as depicted on the Figure 4.1.

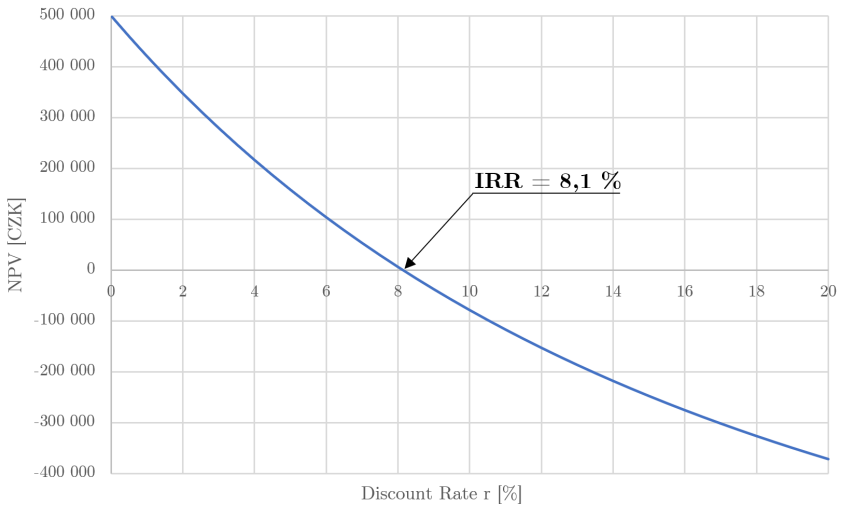

Figure 4.1: This project costs 1 000 000 CZK and then produces cash inflows of 150 000 CZK for 10 years. Its internal rate of return (IRR) is 8,1%, the rate of discount at which NPV is zero.

The project or investment should be accepted or taken into the consideration if it's discount rate or opportunity cost is less than IRR, because in that case the value of NPV is positive. An additional statistics was also provided by the [43] and displayed on Figure 4.2.

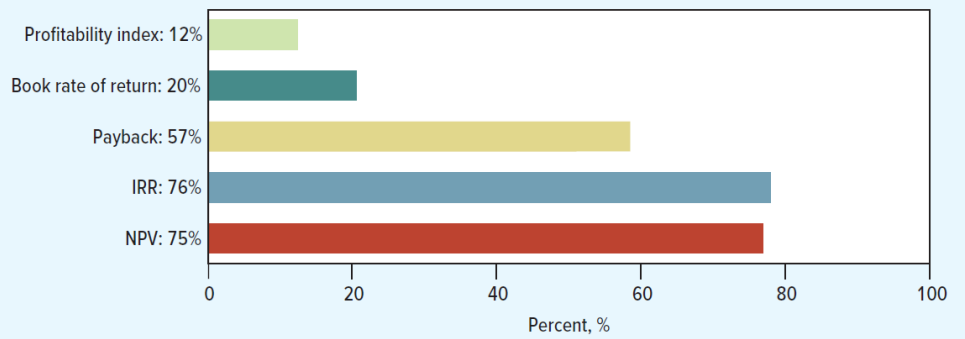

Figure 4.2: *Survey evidence on the percentage of chief financial officers who always, or almost always, use a particular technique for evaluating investment projects.*[43]

4.1.3 Equivalent Annual Cost

Equivalent annual cost is a useful method for comparing investment projects with different lengths of economic life. This method distributes the discounted cash flows over the period of economic life of the investment, so that the cash flows in respective years are equal. In other terms the EAC can be expressed as following:

$$EAC = a \times NPV, \tag{4.4}$$

$$a = \frac{(1+r)^n \times r}{(1+r)^n - 1}, \tag{4.5}$$

where a, n and r are an annuity factor, a length of investment's economic life and the discount rate, respectively. *An annuity is an asset that pays a fixed sum each year for a specified number of years*[43]. The annuity factor illustrates the present value of a money unit a year for each of n years[43]. The project which has lower value of EAC is considered to be better than the other one.

4.1.4 WACC

One of the difficulties in evaluating the economic profitability of investment projects via NPV is to determine the discount rate, that is greatly affected by the risks of the project and other hardly predictable events. In this thesis, one of the widely used financial tools, weighted average cost of capital (WACC), will be used to define the discount rate. WACC is used for capital budgeting analysis, firm valuation and other applications[44]. Additionally, WACC can be used to define the discount rate and can be obtained using the following equation[45]:

$$WACC = \frac{k_e \cdot E + k_d \cdot D \cdot (1-t)}{E + D}, \tag{4.6}$$

where k_e, E, k_d, D and t are cost of equity, level of equity, cost of debt, level of debt and tax rate, respectively. The parameters such as E, D and t can be found online on stock-analysing pages. The data for Eaton company will be taken from [46, 47] and the value of the tax rate will be equal to the Czech Republic's VAT rate:

- E = \$19,04 Billion
- D = \$9,8 Billion
- t = 21 %
- k_e = 11.75 %
- k_d = 6.15 %

The resultant WACC will be calculated for the whole corporation and is equal to 9,41 %. This value will be used as a discount rate for analysis later.

4.2 Theoretical Scenarios

In order to make the analysis as detailed as possible, multiple scenarios will be analyzed: energy compensation by the PV, without any compensation, peak-shaving using the BESS and the PV and peak-shaving using only BESS during the seasons with low sun irradiation. Additionally, the tables with the breakdowns of electricity supply later in the text will include values highlighted with a red color, to make it easier to compare the differences between individual tables.

4.2.1 No Compensation

For a reference May 2023 month will be chosen for the analysis. On this month the value of the consumed energy is equal to 38,91 MWh. According to the calculations from the Table 4.2 the expenses for the energy for this month were equal to 257 372 CZK. As it can be seen from the table, the breakdown of electricity supply includes two positions of reserved capacities, one monthly and one annual. The level of annual reserved capacity is being set at the beginning of each year and cannot be changed throughout the year. The monthly reserved capacity can be changed by the building's operator at the beginning of each month, to better align the reserved monthly capacity with expected maximum of consumption. Usually, annual reserved capacity is higher than monthly, to avoid unpredicted peaks of consumption.

4.2.2 PV Compensation

The idea behind this type of compensation is to simply decrease the amount of consumed energy with the energy that was generated with a help of the solar panels. The average power profiles for this month are displayed on the

Breakdown of electricity supply and regulated services			May-23	
	Number of units	Unit	Rate CZK/Unit	Total CZK
Power electricity	38,91	MWh	3 470	135 018
electricity tax	38,91	MWh	28	1 101
Electricity trade				136 119
Use of distribution networks	38,91	MWh	117	4 568
Unsolicited supply of reactive energy	0,008	MVArh	440	4
Reserved monthly capacity	0,09	MW	224 120	20 171
Annual reserved capacity	0,12	MW	202 480	24 298
Distribution services PREdistribuce, a. s.				49 039
Activities of the market operator	1	month	4	4
Support of electric from the supported energy source	38,91	MWh	495	19 260
System services	38,91	MWh	212	8 281
Regulated Services				27 545
Electricity and regulated services in total without VAT				212 704
VAT rate				% 21
VAT CZK				44 668
Total				257 372

Table 4.2: Breakdown of electricity supply and regulated services for May 2023 (No Compensation).

Figure 4.3. The amount of energy that was generated via the PV during May 2023 is equal to 1,93 MWh. According to the Table 4.3 the expenses associated with the energy consumption are equal to 247 275 CZK.

Breakdown of electricity supply and regulated services			May-23	
	Number of units	Unit	Rate CZK/Unit	Total CZK
Power electricity	36,98	MWh	3 470	128 320
electricity tax	36,98	MWh	28	1 046
Electricity trade				129 367
Use of distribution networks	36,98	MWh	117	4 341
Unsolicited supply of reactive energy	0,008	MVArh	440	4
Reserved monthly capacity	0,09	MW	224 120	20 170
Annual reserved capacity	0,12	MW	202 480	24 297
Distribution services PREdistribuce, a. s.				48 813
Activities of the market operator	1	month	4	4
Support of electric from the supported energy source	36,98	MWh	495	18 305
System services	36,98	MWh	212	7 870
Regulated Services				26 179
Electricity and regulated services in total without VAT				204 359
VAT rate				% 21
VAT CZK				42 915
Total				247 275

Table 4.3: Breakdown of electricity supply and regulated services for May 2023 (PV Compensated).

Moreover, this type of energy compensation does not lower the level of reserved capacity. Hence, the expenses on the distribution services are not lowered.

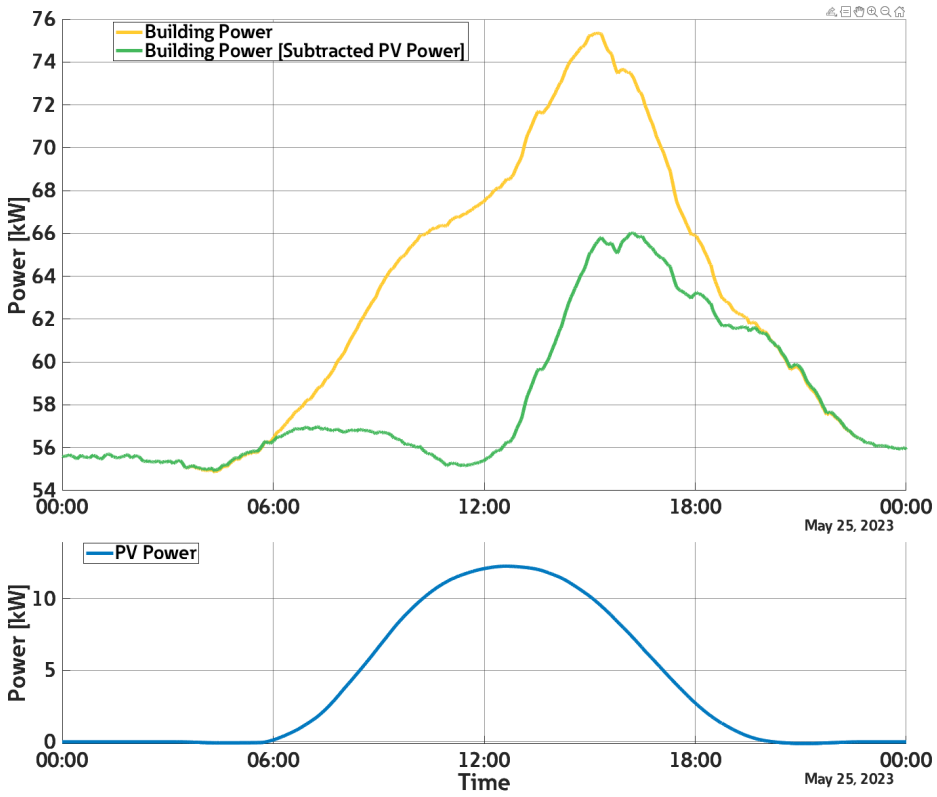

Figure 4.3: Average power profile of the DC MG for May 2023 (PV Compensation).

4.2.3 BESS Compensation

BESS compensation is type of compensation when only BESS is used for the compensation. This approach can be applied during the period when the sun irradiation is low, e.g. in winter. As a reference December 2022 was chosen with an average profile for this month displayed on the Figure 4.4.

Figure 4.4 illustrates BESS's possibility to compensate E_{comp}, which is roughly equal to 50 kWh. Moreover the E_{chrg} roughly equals to 50 kWh, which is enough to charge the BESS during the non-peak hours and do not exceed power consumption level. This compensation allows to lower the reserved power capacity from 62 kW to 54 kW. Tables 4.4 and 4.5 display the total expenses for the energy without and with the described compensation.

Even though it was mentioned that the reserved power capacity can be lowered from 62 kW to 54 kW, it can be seen from the tables that the level of the reserved capacities is slightly higher. This increase in calculations is made due to considerations of reserve space in case of unexpected increase in power consumption.

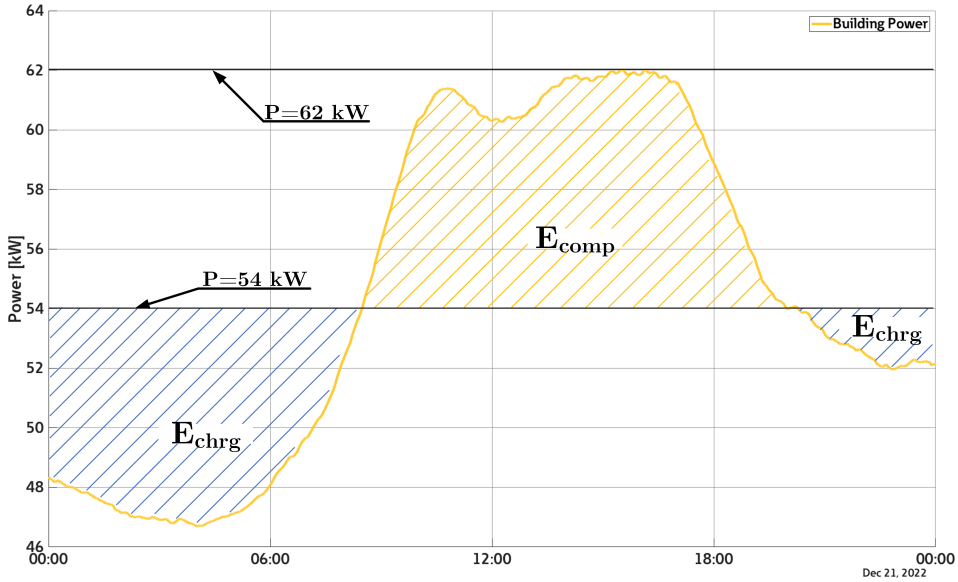

Figure 4.4: Average power profile of the DC MG for December 2022.

Breakdown of electricity supply and regulated services			Dec-22	
	Number of units	Unit	Rate CZK/Unit	Total CZK
Power electricity	38,38	MWh	3 470	133 173
electricity tax	38,38	MWh	28	1 086
Electricity trade				134 260
Use of distribution networks	38,38	MWh	117	4 505
Unsolicited supply of reactive energy	0,008	MVArh	440	4
Reserved monthly capacity	0,08	MW	224 120	17 930
Annual reserved capacity	0,12	MW	202 480	24 298
Distribution services PREdistribuce, a. s.				46 736
Activities of the market operator	1	month	4	4
Support of electric from the supported energy source	38,38	MWh	495	18 997
System services	38,38	MWh	212	8 168
Regulated Services				27 169
Electricity and regulated services in total without VAT				208 165
VAT rate				% 21
VAT CZK				43 715
Total				251 879

Table 4.4: Breakdown of electricity supply and regulated services for December 2022 (No Compensation).

4.2.4 Peak-Shaving

The basic objective of the peak-shaving compensation is to lower the maximum power during the specified time period in order to save costs on the reserved power. In other words, peak-shaving is a combination of the BESS and PV compensations. Considering the same day profile in May 2023, it can be seen from the Figure 4.5 that the PV generation in combination with the BESS could fully shave the day peak and lower the level of the maximum power for this month. On this figure the area highlighted in red is the energy utilized for charging the BESS, whereas the green area is the energy compensated

Breakdown of electricity supply and regulated services			Dec-22	
	Number of units	Unit	Rate CZK/Unit	Total CZK
Power electricity	38,38	MWh	3 470	133 173
electricity tax	38,38	MWh	28	1 086
Electricity trade				134 260
Use of distribution networks	38,38	MWh	117	4 505
Unsolicited supply of reactive energy	0,008	MVArh	440	4
Reserved monthly capacity	0,06	MW	224 120	13 447
Annual reserved capacity	0,07	MW	202 480	16 198
Distribution services PREdistribuce, a. s.				34 154
Activities of the market operator	1	month	4	4
Support of electric from the supported energy source	38,38	MWh	495	18 997
System services	38,38	MWh	212	8 168
Regulated Services				27 169
Electricity and regulated services in total without VAT				195 583
VAT rate				% 21
VAT CZK				41 072
Total				236 656

Table 4.5: Breakdown of electricity supply and regulated services for December 2022 (With Compensation).

by the BESS. The resultant calculations of the expenses are showed in the Table 4.6 and the total expenses for energy are equal to 229 339 CZK.

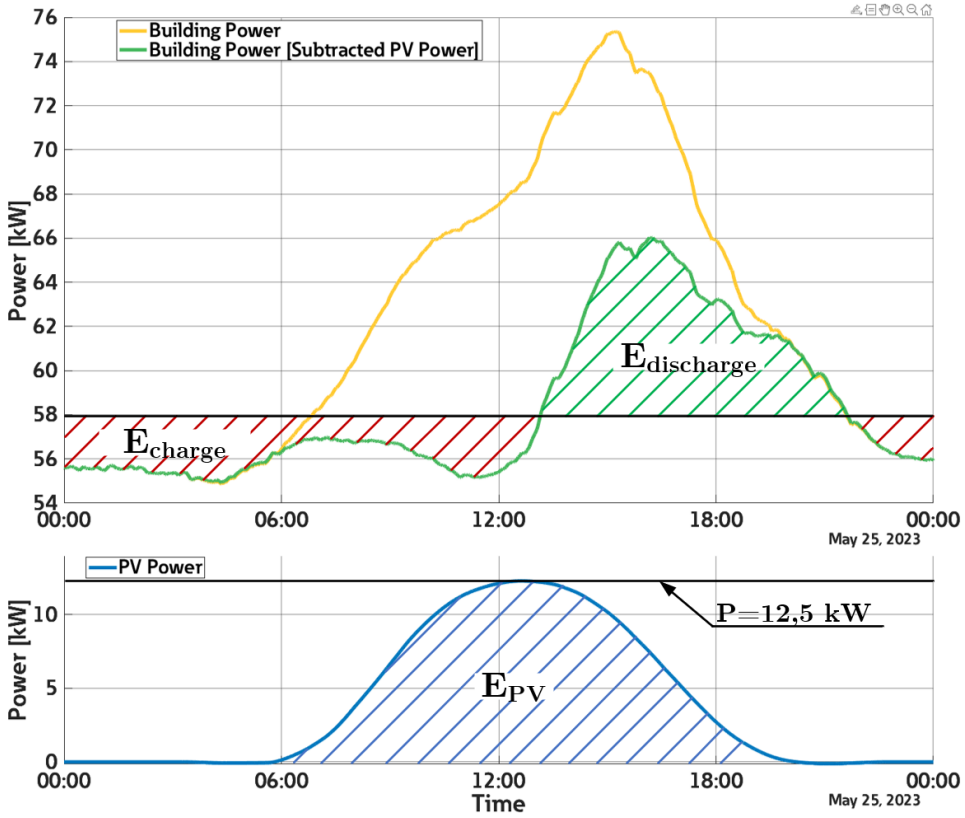

Figure 4.5: Average power profile of the DC MG for May 2023 (Peak-Shaving).

Breakdown of electricity supply and regulated services			May-23	
	Number of units	Unit	Rate CZK/Unit	Total CZK
Power electricity	36,98	MWh	3 470	128 321
electricity tax	36,98	MWh	28	1 047
Electricity trade				129 367
Use of distribution networks	36,98	MWh	117	4 341
Unsolicited supply of reactive energy	0,008	MVArh	440	4
Reserved monthly capacity	0,06	MW	224 120	13 447
Annual reserved capacity	0,08	MW	202 480	16 198
Distribution services PREdistribuce, a. s.				33 990
Activities of the market operator	1	month	4	4
Support of electric from the supported energy source	36,98	MWh	495	18 305
System services	36,98	MWh	212	7 870
Regulated Services				26 179
Electricity and regulated services in total without VAT				189 537
VAT rate				% 21
VAT CZK				39 803
Total				229 339

Table 4.6: Breakdown of electricity supply and regulated services for May 2023 (Peak-Shaving).

Additionally, it was assumed that the peak-shaving compensation could substantially lower the level of both reserved capacities, annual and monthly. In the table it can be seen that the building's operator could specify the annual reserved capacity at a level of 80 kW and the monthly reserved capacity at a level 60 kW. The level of monthly reserved capacity was chosen because of the capability of the PV and the BESS to compensate E_{comp}, which roughly equals to 130 kWh, from the Figure 4.5.

4.3 Evaluation

The economic impact of compensations can be evaluated using combination of economic indicators such as NPV, EAC or IRR. Before analyzing through these methods, it is necessary to define an approximate value of savings associated with the compensating control. Table 4.7 presents calculations made to estimate savings, where $E_{TotBAvrg}$ and $E_{TotPVAvrg}$ represent the total average energy consumed by the building and the total average energy generated via PV during the month in the specified season. The data for these energy values were derived from Table 3.2 in the previous chapter. Savings achieved through peak-shaving for individual months during summer and spring were calculated as the difference between expenses with no compensation and expenses with peak-shaving compensation. Savings for individual months during winter and autumn were calculated as the difference between expenses with no compensation and expenses with BESS compensation. Savings achieved through PV compensation for individual months were calculated as the difference between expenses with no compensation and expenses with PV compensation. Total annual savings amount to 51 216 CZK. Total annual savings achieved with peak-shaving compensation were calculated as the sum of savings for individual months, amounting to 295 843 CZK.

			Expenses/Month [CZK]			
Season	$E_{TotBAvrg}$ [MWh]	$E_{TotPVAvrg}$ [MWh]	No Comp.	PV Comp.	BESS Comp.	Peak-Shave
Summer	39,44	1,41	260 162	252 803	237 579	232 417
Autumn	37,62	0,38	250 606	248 600	233 377	228 215
Winter	37,82	0,15	251 669	250 885	235 661	230 499
Spring	37,58	1,32	250 431	243 508	228 285	223 123
Gross annual savings [CZK]:			0	51 216	233 901	295 843

Table 4.7: Calculation of total savings.

Additionally it is needed to define specific parameters for BESS and PV, such as length of economic life and amount of investments. The investments for BESS and PV are equal to 500 000 CZK and 1 000 000 CZK, respectively. The data about those investments were taken from the company's internal materials. Due to the fact, that the datasheet of the BESS[42] does not specify the exact value for its calendar life, the warranty period, which is equal to 10 years, will be selected for the analysis. Additionally, the datasheet of the PV specify the guaranteed power performance equal to 25 years, which will selected for the analysis. Finally, after considering all needed parameters the NPV analysis can be conducted and the results are shown in the Table 4.8.

	PV	BESS
Investments [CZK]	1 000 000	500 000
Economic Life [Years]	25	10
Discount Rate [%]	9,41	9,41
Annuity Factor [-]	0,11	0,16
Constant Payment [CZK]	105 193	79 316

Table 4.8: Financial parameters for analysis.

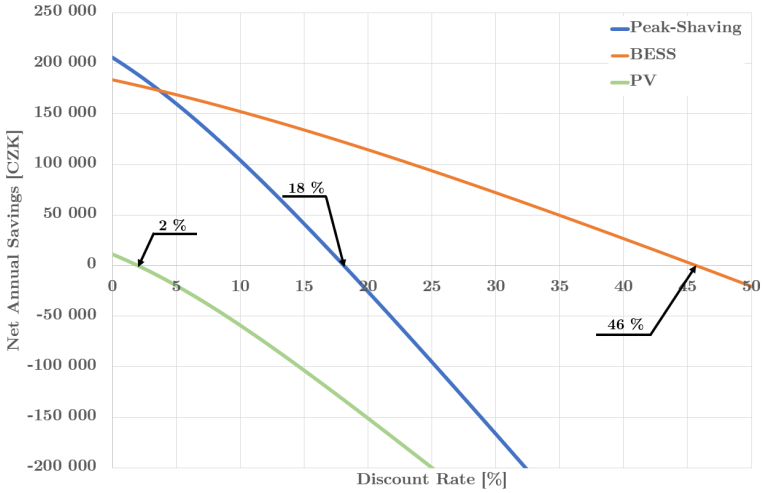

Figure 4.6: Graph of the dependency.

The constant payment in the table represents the equal annual cash flow obtained by multiplying the amount of investments by the annuity factor. This approach allows for the examination of cash flows in individual years,

compensating difficulties that arise because of the different economic life of the technologies and the inclusion of annual savings in the calculations. From the table, it can also be observed that the total gross annual savings achieved with PV compensation are substantially lower than constant payments, indicating that sole PV compensation is not economically effective.

Figure 4.6 depicts the dependency of the net annual savings after subtracting equal constant payments for PV and BESS from the gross annual savings. The calculations of net annual savings do not include the operational expenses, because it was not possible to define them at the moment of writing this study. Hence, it should be noted that inclusion of operational expenses would definetly affect end calculations. From the graph, it can be deduced that the investment into BESS compensation would be economically effective if the discount rate was lower than 46 %. Moreover, the investment into peak-shaving compensation could be beneficial if the discount rate is lower than 18 %.

Chapter 5

Conclusion

In summary, this research has explored various control techniques for microgrids. The initial investigation examined distributed energy resources and existing control techniques. The control techniques which were found are derived from the power control technique that was originally utilized in synchronous generators balancing. Two of the found approaches are aimed at mitigating disadvantages of the conventional control, such as slow transient response and bad performance when RES are integrated.

The DC Microgrid that is examined in this study was comprehensively described, with an accompanying figures and tables for better perception. Moreover, the energy balance was analyzed. It was shown how the microgrid's central controller provides an ability to monitor the data. Additionally, it was found that almost 9 MWh of energy is theoretically lost due to wrongly implemented low-level algorithms in the converter. Moreover, the energy balance analysis showed the theoretical peak-shaving control could be utilized to lower the level of reserved power capacity from 73 kW to 55 kW, with a 50 kWh energy storage system on board.

For the sake of comfortable implementation of the solutions for parameters improvements a simulation of a simplified electrical circuit for the examined DC microgrid was created. The voltage profiles in the simulation were created to be as close to the profiles from the real examined DC MG, with a slight deviation of voltage levels, that didn't affect the overall result.

Voltage drop compensation in DC microgrids was addressed, with a focus on mitigating the voltage drop without considering the cables' inductance. One key aspect of the proposed compensation method is its reliance on values of cables' resistivity, cross-section area, and length. By measuring an approximate value of cables' lengths, cross-section area and cable types in the examined DC MG it was found with a use of formula for conductor's resistance that the cables' resistances vary from 6 $m\Omega$ to 193 $m\Omega$. During the real-life tests of the proposed solution, with a use of the created human-machine interface it was discovered that the voltage drops can be almost $2\,V$ at a current of $10\,A$. However, the proposed approach necessitates defining cables' parameters with sufficient precision to ensure effective compensation. Future research should explore methods to accurately determine these parameters, possibly through advanced measurement techniques.

Meanwhile, measurements' filtering improved data quality, enhancing control precision, during experimentation, an unexpected error offset was encountered in the resultant measurements' filtering process. This offset lowers all of the resultant measurements by $0.5\,V$. Upon author's opinion, this offset is attributed to the impulse response of the proposed filter. Moreover, a workaround was implemented to minimize slow reaction time of the filter during rapid changes. The filtering without the proposed workaround needed around 10 seconds to adjust to big spikes, which was most probably caused by the low sampling period of the filter and measurements. However, further investigation is warranted to optimize the filtering process. Future studies could explore alternative filter designs such as Bessel, Butterworth, or Chebyshev filters to improve accuracy and performance.

Finally, an economic evaluation of the theoretical optimization control algorithm revealed significant benefits. Two average power profiles for two seasons, summer and winter, were comprehensively analysed in terms of energy costs. Based on this analysis the gross annual savings were calculated for the economic evaluation. For instance, the investments into sole photovoltaic compensation of energy could bring savings only in case of discount rate being less than 2 %. The investments into peak-shaving compensation showed the economic effectiveness only in case of discount rate being less than 18 %. Then, the investments to compensation with a use of battery energy storage system displayed the most net annual savings and the effectivness in case of discount rate being less than 46 %. The discount rate for this compensation project was calculated using WACC method and equal to 9.41 %. With a defined discount rate it was found that the net annual savings for BESS compensation are equal to $154\,585\,CZK$, whereas peak-shaving compensation brings $111\,335\,CZK$ of net annual savings. However, there is room for improvement, particularly in the granularity of the analysis. Analyzing the economic impact on a monthly basis could provide more detailed insights into the cost-effectiveness of the proposed solution, allowing for better decision-making and resource allocation in DC microgrid implementation and management. This thesis underscores the intersection of technology and economics, emphasizing the potential for intelligent algorithms to drive greener, more efficient microgrids.

Appendix A

Nomenclature

Symbol	Meaning
$P-\omega$	Active Power - Frequency
$Q-E$	Reactive Power - Voltage
V_{OC}	Opec-Circuit Voltage
AC	Alternating Current
BESS	Battery Energy Storage System
DC	Direct Current
DC MG	DC Microgrid
DER	Distributed Energy Resources
EAC	Equivalent Annual Cost
ESS	Energy Storage System
EV	Electric Vehicle
FIR	Finite Impulse Response
HMI	Human Machine Interface
HVDC	High Voltage Direct Current
LV	Low Voltage
LVDC	Low Voltage Direct Current
MG	Microgrid
MGCC	Microgrid Central Controller
MV	Medium Voltage
MVAC	Medium Voltage Alternating Current
NPV	Net Present Value
PCC	Point of Common Coupling
PQ	Power Quality
PV	Photovoltaic
R&D	Research & Development
RES	Renewable Energy Source
SG	Smart-grids

Appendix B

Figures

Appendix C

Tables

Appendix D

Bibliography

[1] S. Solomon, G.-K. Plattner, R. Knutti, and P. Friedlingstein, "Irreversible climate change due to carbon dioxide emissions," *Proceedings of the National Academy of Sciences*, vol. 106, pp. 1704–1709, Feb. 2009.

[2] "United Nations Development Programme." `https://www.undp.org/sustainable-development-goals/affordable-and-clean-energy`. Accessed: November 14, 2023.

[3] H. Ritchie, M. Roser, and P. Rosado, "Energy," *Our World in Data*, 2022. https://ourworldindata.org/energy.

[4] "Fact Sheets on the European Union." `https://www.europarl.europa.eu/factsheets/en/sheet/68/energy-policy-general-principles`. Accessed: November 14, 2023.

[5] C. Cecati, G. Mokryani, A. Piccolo, and P. Siano, "An overview on the smart grid concept," in *IECON 2010 - 36th Annual Conference on IEEE Industrial Electronics Society*, pp. 3322–3327, 2010.

[6] T. Dragicevic, J. C. Vasquez, J. M. Guerrero, and D. Skrlec, "Advanced lvdc electrical power architectures and microgrids: A step toward a new generation of power distribution networks," *IEEE Electrification Magazine*, vol. 2, no. 1, pp. 54–65, 2014.

[7] R. Lasseter, "Microgrids," in *2002 IEEE Power Engineering Society Winter Meeting. Conference Proceedings (Cat. No.02CH37309)*, vol. 1, pp. 305–308 vol.1, 2002.

[8] F. Perez, A. Iovine, G. Damm, and P. Ribeiro, "Dc microgrid voltage stability by dynamic feedback linearization," in *2018 IEEE International Conference on Industrial Technology (ICIT)*, pp. 129–134, 2018.

[9] S. Bagheri and H. M. CheshmehBeigi, "Dc microgrid voltage stability through inertia enhancement using a bidirectional dc-dc converter," in *7th Iran Wind Energy Conference (IWEC2021)*, pp. 1–5, 2021.

[10] "Large Language Model, ChatGPT 3.5." `https://chat.openai.com/`. Accessed: May 2, 2024.

[11] M. F. Akorede, H. Hizam, and E. Pouresmaeil, "Distributed energy resources and benefits to the environment," *Renewable and Sustainable Energy Reviews*, vol. 14, p. 724–734, Feb. 2010.

[12] Şiir Kılkış, G. Krajačić, N. Duić, M. A. Rosen, and M. A. Al-Nimr, "Advances in integration of energy, water and environment systems towards climate neutrality for sustainable development," *Energy Conversion and Management*, vol. 225, p. 113410, Dec. 2020.

[13] N. Kannan and D. Vakeesan, "Solar energy for future world: - a review," *Renewable and Sustainable Energy Reviews*, vol. 62, p. 1092–1105, Sept. 2016.

[14] R. A. Marques Lameirinhas, J. P. N. Torres, and J. P. de Melo Cunha, "A photovoltaic technology review: History, fundamentals and applications," *Energies*, vol. 15, p. 1823, Mar. 2022.

[15] J. Ascencio-Vásquez, J. C. Osorio-Aravena, K. Brecl, E. Muñoz-Cerón, and M. Topič, "Typical daily profiles, a novel approach for photovoltaics performance assessment: Case study on large-scale systems in chile," *Solar Energy*, vol. 225, p. 357–374, Sept. 2021.

[16] R. Yao and K. Steemers, "A method of formulating energy load profile for domestic buildings in the uk," *Energy and Buildings*, vol. 37, p. 663–671, June 2005.

[17] A. Joseph and M. Shahidehpour, "Battery storage systems in electric power systems," in *2006 IEEE Power Engineering Society General Meeting*, IEEE, 2006.

[18] N. Hatziargyriou, H. Asano, R. Iravani, and C. Marnay, "Microgrids," *IEEE Power and Energy Magazine*, vol. 5, p. 78–94, July 2007.

[19] J. J. Justo, F. Mwasilu, J. Lee, and J.-W. Jung, "Ac-microgrids versus dc-microgrids with distributed energy resources: A review," *Renewable and Sustainable Energy Reviews*, vol. 24, p. 387–405, Aug. 2013.

[20] N. Lidula and A. Rajapakse, "Microgrids research: A review of experimental microgrids and test systems," *Renewable and Sustainable Energy Reviews*, vol. 15, p. 186–202, Jan. 2011.

[21] M. Hatti, A. Meharrar, and M. Tioursi, "Power management strategy in the alternative energy photovoltaic/pem fuel cell hybrid system," *Renewable and Sustainable Energy Reviews*, vol. 15, p. 5104–5110, Dec. 2011.

[22] S. Paul, A. Tamrakar, and N. P. Padhy, "Demand side management based optimal scheduling portfolio of a microgrid in linear programming platform," in *2018 20th National Power Systems Conference (NPSC)*, pp. 1–6, 2018.

[23] Y. W. Li and C.-N. Kao, "An accurate power control strategy for power-electronics-interfaced distributed generation units operating in a low-voltage multibus microgrid," *IEEE Transactions on Power Electronics*, vol. 24, no. 12, pp. 2977–2988, 2009.

[24] M. H. Saeed, W. Fangzong, B. A. Kalwar, and S. Iqbal, "A review on microgrids' challenges & perspectives," *IEEE Access*, vol. 9, p. 166502–166517, 2021.

[25] L. Ahmethodzic and M. Music, "Comprehensive review of trends in microgrid control," *Renewable Energy Focus*, vol. 38, p. 84–96, Sept. 2021.

[26] T. L. Vandoorn, B. Meersman, L. Degroote, B. Renders, and L. Vandevelde, "A control strategy for islanded microgrids with dc-link voltage control," *IEEE Transactions on Power Delivery*, vol. 26, p. 703–713, Apr. 2011.

[27] A. Mohd, E. Ortjohann, D. Morton, and O. Omari, "Review of control techniques for inverters parallel operation," *Electric Power Systems Research*, vol. 80, p. 1477–1487, Dec. 2010.

[28] P. Borazjani, N. I. A. Wahab, H. B. Hizam, and A. B. C. Soh, "A review on microgrid control techniques," in *2014 IEEE Innovative Smart Grid Technologies - Asia (ISGT ASIA)*, pp. 749–753, 2014.

[29] U. B. Tayab, M. A. B. Roslan, L. J. Hwai, and M. Kashif, "A review of droop control techniques for microgrid," *Renewable and Sustainable Energy Reviews*, vol. 76, p. 717–727, Sept. 2017.

[30] L. Gomez, L. Lourenço, M. Salles, A. Grilo, and A. Filho, *Frequency support by grid connected DFIG-based wind farms*, p. 481–496. Elsevier, 2021.

[31] M. Chandorkar, D. Divan, and R. Adapa, "Control of parallel connected inverters in standalone ac supply systems," *IEEE Transactions on Industry Applications*, vol. 29, no. 1, pp. 136–143, 1993.

[32] J.-W. Kim, H.-S. Choi, and B. H. Cho, "A novel droop method for converter parallel operation," *IEEE Transactions on Power Electronics*, vol. 17, no. 1, pp. 25–32, 2002.

[33] S. Anand, B. G. Fernandes, and J. Guerrero, "Distributed control to ensure proportional load sharing and improve voltage regulation in low-voltage dc microgrids," *IEEE Transactions on Power Electronics*, vol. 28, no. 4, pp. 1900–1913, 2013.

[34] J. Kumar, A. Agarwal, and V. Agarwal, "A review on overall control of dc microgrids," *Journal of Energy Storage*, vol. 21, p. 113–138, Feb. 2019.

[35] A. Iovine, S. B. Siad, G. Damm, E. De Santis, and M. D. Di Benedetto, "Nonlinear control of a dc microgrid for the integration of photovoltaic panels," *IEEE Transactions on Automation Science and Engineering*, vol. 14, no. 2, pp. 524–535, 2017.

[36] B. Modu, M. P. Abdullah, M. A. Sanusi, and M. F. Hamza, "Dc-based microgrid: Topologies, control schemes, and implementations," *Alexandria Engineering Journal*, vol. 70, p. 61–92, May 2023.

[37] R. H. Lasseter, Z. Chen, and D. Pattabiraman, "Grid-forming inverters: A critical asset for the power grid," *IEEE Journal of Emerging and Selected Topics in Power Electronics*, vol. 8, no. 2, pp. 925–935, 2020.

[38] "Photovoltaic Geographical Information System." `https://re.jrc.ec.europa.eu/pvg_tools/en/`. Accessed: March 12, 2024.

[39] D. Sundararajan, *Finite Impulse Response Filters*, p. 189–249. Springer International Publishing, 2021.

[40] "CoDeSys Forge Forum." `https://forge.codesys.com/forge/talk/CODESYS-V2/thread/9d72ee0891/`. Accessed: April 7, 2024.

[41] "Solar Panels Datasheet." `https://web.archive.org/web/20161108155354/http://www.jinkosolar.com/ftp/EN-JKM270P-60(4BB).pdf`. Accessed: April 14, 2024.

[42] "Battery Packs Datasheet." `https://www.eaton.com/content/dam/eaton/products/energy-storage/xstorage-compact/en-us/eaton-xstorage-compact-technical-datasheet-en-us.pdf`. Accessed: April 14, 2024.

[43] R. A. Brealey, *Principles of corporate finance*. McGraw-Hill Higher Education; 14th edition, 2023.

[44] R. Rehman and A. Raoof, "Weighted average cost of capital (wacc) traditional vs new approach for calculating the value of firm," *International Research Journal of Finance and Economics*, vol. 45, pp. 7–9, 2010.

[45] I. Guaita-Pradas and A. Blasco-Ruiz, "Analyzing profitability and discount rates for solar pv plants. a spanish case," *Sustainability*, vol. 12, p. 3157, Apr. 2020.

[46] "Eaton Stock Analysis." `https://stockanalysis.com/stocks/etn/statistics/`. Accessed: April 21, 2024.

[47] "Toolbox for Market Analysis." `https://finbox.com/NYSE:ETN/models/wacc`. Accessed: April 27, 2024.

Appendix E

Attachments

```
    PROGRAM VoltageDropCompensation
VAR
    CableResistanceBAT: REAL;
    CableResistancePV: REAL;
    CableResistanceAFE: REAL;
    ConnCableResistance: REAL;
    V_DropPV: REAL;
    V_DropBAT: REAL;
    V_DropAFE: REAL;
    CurrentBAT: REAL;
    CurrentPV: REAL;
    CurrentAFE: REAL;
END_VAR

HMI_VoltagePV(F := Upv.F, Q := 0);
HMI_VoltageBAT(F := BAT_Zeka_U_BHi.F, Q := 0);
HMI_VoltageAFE(F := Uafedc.F, Q := 0);
CurrentBAT := BAT_Zeka_I_BHi.F;
CurrentPV := Ipv.F;
CurrentAFE := Iafedc.F;

// Resistances of the DC-bus lines:
IF HMI_CableCrossSection.F <> 0 THEN
    CableResistanceBAT := 2 * HMI_CableResistivity.F *...
    EXPT(10, -8) * HMI_CableLengthBattery.F /...
    (HMI_CableCrossSection.F * EXPT(10, -6));

    CableResistancePV := 2 * HMI_CableResistivity.F *...
    EXPT(10, -8) * HMI_CableLengthPV.F /...
    (HMI_CableCrossSection.F * EXPT(10, -6));

    CableResistanceAFE := 2 * HMI_CableResistivity.F *...
    EXPT(10, -8) * HMI_CableLengthAFE.F /...
    (HMI_CableCrossSection.F * EXPT(10, -6));
```

```
    // Resistance of the connecting cables:
    ConnCableResistance := 2 * HMI_CableResistivity.F *...
    EXPT(10, -8) * 2 / (HMI_CableCrossSection.F *...
    EXPT(10, -6));
END_IF

// Calculation of voltage drops for individual devices:
HMI_VoltageDropPV(F := CurrentPV * (ConnCableResistance +...
CableResistancePV), Q := 0);

HMI_VoltageDropBAT(F := CurrentBAT * (ConnCableResistance +...

CableResistanceBAT), Q := 0);

HMI_VoltageDropAFE(F := CurrentAFE * (ConnCableResistance +...

CableResistanceAFE), Q := 0);

// Voltage drop compensation:
HMI_VoltagePV_Comp(F:=HMI_VoltagePV.F+...
HMI_VoltageDropPV.F,Q:=0);

HMI_VoltageBAT_Comp(F:=HMI_VoltageBAT.F+...
HMI_VoltageDropBAT.F,Q:=0);

HMI_VoltageAFE_Comp(F:=HMI_VoltageAFE.F+...
HMI_VoltageDropAFE.F,Q:=0);
```

Code E.1: Program for voltage drop compensation on MGCC

```
(*
*
* File: Gritsyuk_SIM_BC_DCMG_2022b_v18.st
*
* IEC 61131-3 Structured Text (ST) code generated for
    subsystem "Gritsyuk_SIM_BC_DCMG_2022b_v18/Modified_FIR"
*
* Model name                      :
    Gritsyuk_SIM_BC_DCMG_2022b_v18
* Model version                   : 1.63
* Model creator                   : Leon Gritsyuk
* Model last modified by          : Leon Gritsyuk
* Model last modified on          : Fri Apr 26 10:11:52 2024
* Model sample time               : 0.0001s
* Subsystem name                  :
    Gritsyuk_SIM_BC_DCMG_2022b_v18/Modified_FIR
* Subsystem sample time           : 2s
```

```
* Simulink PLC Coder version      : 3.7 (R2022b) 13-May-2022
* ST code generated on            : Fri Apr 26 10:12:22 2024
*
* Target IDE selection            : 3S CoDeSys 3.5
* Test Bench included             : No
*
*)
FUNCTION_BLOCK Modified_FIR
VAR_INPUT
    ssMethodType: SINT;
    inputSignal: LREAL;
END_VAR
VAR_OUTPUT
    filteredSignal: LREAL;
END_VAR
VAR
    DiscreteFIRFilter_circBuf: DINT;
    DiscreteFIRFilter: LREAL;
    Delay6_DSTATE: LREAL;
    Delay7_DSTATE: LREAL;
    DiscreteFIRFilter_states: ARRAY [0..23] OF LREAL;
    c_DiscreteFIRFilter_Coeffic: ARRAY [0..24] OF LREAL :=
    0.00036490343398085491,0.0013368060424696758,
    0.0034793853527283034,0.0073906009386682176,
    0.013630426098342483,0.022537846332198602,
    0.0340536701151822,0.047598560026536348,
    0.0620577947297915,0.07590043068702032,
    0.087423176160264029,0.095069873135326888,
    0.09774952254386135,0.095069873135326888,
    0.087423176160264029,0.07590043068702032,
    0.0620577947297915,0.047598560026536348,
    0.0340536701151822,0.022537846332198602,
    0.013630426098342483,0.0073906009386682176,
    0.0034793853527283034,0.0013368060424696758,
    0.00036490343398085491;
END_VAR
VAR_TEMP
    j: DINT;
    clock_OUT: LREAL;
    i: DINT;
END_VAR
CASE ssMethodType OF
    SS_INITIALIZE:
        (* SystemInitialize for Atomic SubSystem: '<Root>/
   Modified_FIR' *)
        (* InitializeConditions for Delay: '<S1>/Delay6' *)
```

```
    Delay6_DSTATE := 0.0;
    (* InitializeConditions for Delay: '<S1>/Delay7' *)
    Delay7_DSTATE := 0.0;
    (* InitializeConditions for DiscreteFir: '<S1>/
Discrete FIR Filter' *)
    DiscreteFIRFilter_circBuf := 0;
    (* End of SystemInitialize for SubSystem: '<Root>/
Modified_FIR' *)
    (* SystemInitialize for Atomic SubSystem: '<Root>/
Modified_FIR' *)
    (* InitializeConditions for DiscreteFir: '<S1>/
Discrete FIR Filter' *)
    FOR i := 0 TO 23 DO
        DiscreteFIRFilter_states[i] := 700.0;
    END_FOR;
    (* End of SystemInitialize for SubSystem: '<Root>/
Modified_FIR' *)
SS_STEP:
    (* Outputs for Atomic SubSystem: '<Root>/Modified_FIR
' *)
    (* DiscreteFir: '<S1>/Discrete FIR Filter' *)
    clock_OUT := inputSignal * 0.00036490343398085491;
    i := 1;
    j := DiscreteFIRFilter_circBuf;
    WHILE j < 24 DO
        clock_OUT := (DiscreteFIRFilter_states[j] *
c_DiscreteFIRFilter_Coeffic[i]) + clock_OUT;
        i := i + 1;
        j := j + 1;
    END_WHILE;
    j := 0;
    WHILE j < DiscreteFIRFilter_circBuf DO
        clock_OUT := (DiscreteFIRFilter_states[j] *
c_DiscreteFIRFilter_Coeffic[i]) + clock_OUT;
        i := i + 1;
        j := j + 1;
    END_WHILE;
    (* DiscreteFir: '<S1>/Discrete FIR Filter' *)
    DiscreteFIRFilter := clock_OUT;
    (* MATLAB Function: '<S1>/MATLAB Function3'
incorporates:
    *  Constant: '<S1>/Constant7'
    *  Delay: '<S1>/Delay6'
    *  Delay: '<S1>/Delay7' *)
    (* MATLAB Function 'Modified_FIR/MATLAB Function3':
'<S2>:1' *)
```

```
        (* '<S2>:1:3' if abs(Voltage_N - Voltage_N_1) > 5 *)
        IF ABS(inputSignal - Delay6_DSTATE) > 5.0 THEN
            (* '<S2>:1:4' clock_OUT = filterOrder; *)
            clock_OUT := 24.0;
        ELSE
            (* '<S2>:1:5' else *)
            (* '<S2>:1:6' clock_OUT = clock_IN - 1; *)
            clock_OUT := Delay7_DSTATE - 1.0;
        END_IF;
        (* '<S2>:1:9' if clock_OUT > 0 *)
        IF clock_OUT > 0.0 THEN
            (* Outport: '<Root>/filteredSignal' *)
            (* '<S2>:1:10' Voltage_OUT = Voltage_N; *)
            filteredSignal := inputSignal;
        ELSE
            (* Outport: '<Root>/filteredSignal' *)
            (* '<S2>:1:11' else *)
            (* '<S2>:1:12' Voltage_OUT = Voltage_FIR; *)
            filteredSignal := DiscreteFIRFilter;
        END_IF;
        (* Update for Delay: '<S1>/Delay6' *)
        Delay6_DSTATE := inputSignal;
        (* Update for Delay: '<S1>/Delay7' incorporates:
        *  MATLAB Function: '<S1>/MATLAB Function3' *)
        Delay7_DSTATE := clock_OUT;
        (* Update for DiscreteFir: '<S1>/Discrete FIR Filter'
     *)
        (* Update circular buffer index *)
        DiscreteFIRFilter_circBuf :=
    DiscreteFIRFilter_circBuf - 1;
        IF DiscreteFIRFilter_circBuf < 0 THEN
            DiscreteFIRFilter_circBuf := 23;
        END_IF;
        (* Update circular buffer *)
        DiscreteFIRFilter_states[DiscreteFIRFilter_circBuf]
    := inputSignal;
        (* End of Update for DiscreteFir: '<S1>/Discrete FIR
    Filter' *)
        (* End of Outputs for SubSystem: '<Root>/Modified_FIR
    ' *)
END_CASE;
END_FUNCTION_BLOCK
VAR_GLOBAL CONSTANT
    SS_INITIALIZE: SINT := 0;
    SS_STEP: SINT := 1;
END_VAR
```

Code E.2: FIR Filter function generated by the Simulink's "PLC-Coder" package.

```
PROGRAM FIR_Filter_BAT
VAR
    filterInstance: Modified_FIR;

    Delay : TON;
END_VAR

Delay(IN:=TRUE, PT:=T#2S);
IF NOT(Delay.Q) THEN
   RETURN;
END_IF
Delay(IN:=FALSE);

filterInstance.ssMethodType := SS_STEP;

filterInstance.measuredSignal := HMI_VoltageBAT.F;
filterInstance();
HMI_VoltageBAT_Filter(F := filterInstance.filteredSignal, Q
    := 0);
```

Code E.3: Implementation of the FIR filter in the MGCC with the delay for the Battery converter $C2$.